A combined laboratory and field-based experimental approach to characterize the heterogeneity of granular aquifers

Lamine Boumaiza[1,2], Romain Chesnaux[2], Randy L. Stotler[1], Alain Rouleau[2], Yan Levesque[2], Okke Batelaan[3], Pierre A. Cousineau[2], Thomas M. Missimer[4]

[1] University of Waterloo, Department of Earth and Environmental Sciences, Waterloo (Ontario), N2T 3G4, Canada

[2] Université du Québec à Chicoutimi, Département des Sciences Appliquées, Saguenay (Québec), G7H 2B1, Canada

[3] Flinders University, College of Science and Engineering, National Centre for Groundwater Research and Training, Adelaide, 5001, Australia

[4] Florida Gulf Coast University, U. A. Whitaker College of Engineering, Fort Myers, FL, 33913, USA

Corresponding author: E-mail address: lamine.boumaiza@uwaterloo.ca (L. Boumaiza)

Abstract

Effective groundwater resource management requires appropriate conceptualization of aquifer heterogeneity, which is challenging for pro-deltaic systems. This study focuses on heterogeneity within the Valin River paleodelta (Canada), a complex granular aquifer constituting a system that is a regional water supply source. This study integrates laboratory and field-based experimental measurements of various hydrogeological properties and classifies the sediments using diverse statistical techniques. It demonstrates the advantage of diversified characterization for a better understanding of aquifer heterogeneity. The hydrogeological properties (i.e., hydraulic conductivity (K) and porosity (n)) of 27 lithofacies identified in nine sandpits were estimated and assigned a range of values. The identified lithofacies were grouped into four operative-lithofacies before assigned to three primary hydrofacies that were used to define the aquifer heterogeneity. The importance of integrated sediment and hydraulic properties assessment is that the techniques allow an understanding of the heterogeneity within a complex pro-deltaic aquifer type. Two scales of heterogeneity are defined: (i) lithofacial scale wherein small differences in sediment

texture (grain size properties), in sedimentary structures, and in other sediment features of lithofacies (mean grain diameter, sorting, skewness, and kurtosis) cause significant changes in K and n, (ii) hydrofacial scale wherein specific lithology units define larger-scale aquifer flow and potential solute movement. The multi-methodology approach used for characterizing the aquifer heterogeneity is a prerequisite to complete necessary information for developing more accurate and complex hydrogeological models.

Keywords
Aquifer properties, Lithofacies, Hydrofacies, Porosity, Hydraulic conductivity, Laboratory experiments

1. Introduction

Granular aquifers are used worldwide as major sources for water supply given their potential to provide appreciable groundwater quantity and quality (Mohammed et al. 2014; Pauloo et al. 2021; Rongier and Peeters 2022). Access to such groundwater has allowed significant social and economic development, but is often accompanied by uncontrolled anthropogenic practices leading to deterioration of groundwater quality (Boumaiza et al. 2020a, 2022a 2022d; Elmeknassi et al. 2022). Effective and sustainable groundwater resource management requires a detailed information on the internal architecture of granular deposits. This detailed information is helpful for multiple implications such as suitable understanding of groundwater flow patterns and contaminant transport (Slomka et al. 2019; De Caro et al. 2020), accurate assessment of groundwater travel time (Boumaiza et al. 2020b), effective design of wellhead protection areas (Rasmussen et al. 2006), and feasibility of managed aquifer groundwater recharge plans (Maples et al. 2019). Several studies show that heterogeneity within porous media on centimetre to decimetre scales significantly influences the spread of contaminants (Iversen et al. 2008; Possemiers et al. 2012; Winiarski et al. 2013). Therefore, neglecting the effect of aquifer heterogeneity could lead to profound implications on groundwater management and contamination potential. In addition, aquifer heterogeneity plays an important role in evaluating the potential spreading rate of various contaminants where longitudinal and transverse dispersivity are critical in the development of plans to remediate contamination (Sun et al. 2008; Yin et al. 2023).

For a better understanding of the internal heterogeneity of fluvial deposits, knowledge about the links between the sediment units and their hydrogeological properties

is required, which has led to sedimentological applications to hydrogeologic problems (Anderson 1989a; Fogg and Zhang 2016; Ma et al. 2017). Several studies demonstrate that sediment hydrogeological properties, such as hydraulic conductivity (K) and porosity (n), are controlled by sedimentological characteristics including the texture, sorting, and structure of sediments (Anderson 1989a). It is clearly understood that well-sorted sediments featuring large grain sizes with a high degree of rounding have higher K values compared to poorly sorted sediments dominated by very fine-grained material (Anderson 1989a; Bierkens and Weerts 1994). Some researchers applied a simple approach to characterize the heterogeneity of aquifers by using sedimentary lithological units (lithofacies); then grouping lithofacies featuring relative homogeneity of hydrogeological properties into hydrofacies (Poeter and Gaylord 1990; Eaton 2006). The challenge is the ability to identify subsurface lithofacies and to accurately characterize their hydrogeological properties.

Subsurface field hydrogeological tests, such as pumping tests can be used to measure aquifer hydraulic properties. However, this assessment involves a much larger aquifer volume than the small-scale sedimentological heterogeneity controlling smaller-scale hydraulic properties. Also, pumping test-based methods generally assume homogeneous and isotropic porous media with uniform thickness of the saturated zone (Theis 1935; De Clercq et al. 2020). These simplifications in most cases do not correspond to the actual distribution of hydraulic properties within most aquifers. Outcrops can be used to identify sediment lithology and to conduct in-situ measurements of hydrogeological properties. This allows developing alternative aquifer analogs to be used in subsurface conceptual models (Huggenberger and Aigner 1999; Lévesque et al. 2023). However,

sedimentary outcrops are often exposed to erosion and diagenetic processes, which can introduce discrepancies between the outcrop lithology and that preserved in the subsurface. Geophysical methods are also used to investigate the internal architecture of granular aquifers (Hinnell et al. 2010; Lévesque et al. 2021). However, these indirect methods can only provide an approximate characterization of subsurface structures, and do not permit an accurate assessment of hydrogeological properties without detailed calibration (Becht et al. 2007; Brauchler et al. 2010). To overcome this shortfall, a number of researchers have adopted small-scale hydrofacies analysis of open operational artificial pits to ascertain the heterogeneity of aquifers at a larger scale (Klingbeil et al. 1999; Heinz and Aigner 2003; Heinz et al. 2003). Open freshly excavated exposures offer easy access to lithofacies, allowing identification of their sedimentological characteristics, and to perform hydrogeological tests (e.g., grain size analyses and hydraulic conductivity measurements at different depths in the stratigraphic section) (Franco et al. 2017).

Klingbeil et al. (1999) investigated a glaciofluvial deposit, in which they linked several different lithofacies, featuring identical K and n, to a unique hydrofacies. Conversely, Zappa et al. (2006) identified several lithofacies with different hydrogeological properties in a case study of an alluvial aquifer, despite the fact that these lithofacies were characterized by the same class and grain size fractions. Similarly, Heinz et al. (2003) and Kostic et al. (2005) showed considerable variability in hydrogeological properties for lithofacies identified in Quaternary gravel deposits. Due to the heterogeneity of natural granular deposits, significant differences in lithofacies hydrogeological properties can be observed (Won et al. 2019; Amiri et al. 2022; Ma et al. 2023). Deltaic deposits usually feature a great diversity of lithofacies (Postma, 1984; Prior et al. 1984;

Maizels 1993; Ouellon et al. 2008), resulting in highly heterogeneous aquifers, where the same lithofacies can be present in more than one location within an aquifer caused by variability in hydrogeological properties. Despite efforts to understand the heterogeneity of aquifers, there are limited studies illustrating the advantage of a multi-methodology approach to better understand the heterogeneity of complex deltaic aquifers.

The present study aims to show the advantage of diversified characterization methods of the lithofacies to better describe the variability of their hydrogeological properties within a pro-deltaic system. This study integrates laboratory and field-based experimental measurements of various hydrogeological features and describes the lithofacies according to diverse statistical techniques. The present study is focused on the aquifers of the Valin River paleodeltaic system in Quebec (Canada). This granular system contains several operational sandpits offering an excellent opportunity to complete sediment-to-aquifer hydrogeological characterization based on a proposed multi-techniques approach. The present study does not investigate the sedimentation processes from the identified lithofacies. The selected Valin River paleodelta system constitutes a major source of water supply under anthropogenic development activities. Hence, understanding the aquifer heterogeneity is expected to contribute to the effective and sustainable management of the aquifer system and its protection.

2. Setting of study area

2.1 Geographic location, physiography and climate conditions

The study area covers a surface area of approximately 60 km^2 and is located in the Saguenay-Lac-Saint-Jean (SLSJ) region of Quebec, Canada (Fig. 1a). It features flat to irregular topography with land surface covered by forest, agricultural lands, urban areas,

and the Saint-Honoré Airport. The study area experiences a humid continental climate, with average monthly temperatures ranging from −16°C in January to +18°C in July. An average annual precipitation of 900 mm occurs over the study area, and is received as both rainfall and snowfall. Precipitation in the summer-autumn seasons is mainly received as rainfall, whereas snowfall is dominating during the winter-spring period ranging from November to March/April (Government of Canada 2022).

2.2 Geological overview

The study area belongs to the SLSJ region, which was marked by the last phase of the Wisconsinan glaciation that ended approximately 7,000 years ago (Parent and Occhietti 1988; Lévesque et al. 2020). During its retreat toward the north, the last glacier covering the SLSJ region left behind a discontinuous/heterogeneous layer of till, several terminal moraines and glaciolacustrine/fluvio-glacial deposits, which were derived from the rock-basement (Lasalle and Tremblay 1978; Pagé 1999; Daigneault et al. 2011). Following glacial retreat, the isostatic depression caused by its weight, combined with a rapid global rise in sea level, led to a marine transgression, and the incursion of the Laflamme Sea into the SLSJ region approximately 12,900 years ago (Nutz et al. 2013, 2015). This resulted in deposition of semi-continuous impermeable clayey silt and silty clay, overlain by post-glacial granular sediments (i.e., prograding littoral/deltaic deposits) that were deposited during the Laflamme Sea regression. In the SLSJ region, the deltaic system of the study area was formed at the mouth of the Valin River that prograded north to south into the post-glacial Laflamme Sea. During the later isostatic rebound, the Valin River bed deepened after the retreat of the Laflamme Sea and cut the deltaic system into two parts, thus, creating

two separate aquifers with one to the west (Saint-Honoré) and the other one to the east (Saint-Fulgence) (Fig. 1b).

The aquifers of the Valin River paleodelta system vary in thickness with a maximum of 50 m. They are mainly constituted of post-glacial Quaternary deposits composed of sand with silt overlying (i) impermeable unconsolidated material from Laflamme Sea transgression, or (ii) directly a Precambrian crystalline bedrock, belonging to the Canadian Shield, with discontinuous Ordovician limestone (cross-section A-A' in Fig. 1c) of variable thickness (Hébert and Lacoste 1998; CERM-PACES 2013).

2.3 Hydrogeological background

The aquifers of the Valin River paleodelta constitute an important groundwater reservoir, supplying 34% of the local demand for domestic, commercial and industrial uses (CERM-PACES 2013). The groundwater recharge was estimated at 60% of the annual precipitation, and occurs mainly during summer-autumn period as the heavy snow accumulation during the winter/fall cold period limits the water infiltration into the subsurface due to the presence of frozen snowpack and ground acting as a barrier to infiltration (Boumaiza et al. 2020c, 2022b). The water table within the Valin River paleodelta system generally varies between 1 and 7 m below ground surface and generally mimics the land surface topography. Groundwater discharges primarily into some local surface water bodies, then drains further into the Saguenay River (Tremblay 2005; Boumaiza 2008; Boumaiza et al. 2021a). The bedrock of the study area has not been well documented, but it has been described for neighboring regions (Chesnaux and Elliott 2011; CERM-PACES 2013). It may be hydraulically connected with the overlying granular deposits through faults and fractures occurring in the upper part of the bedrock. The granular deposits and fractured-

rock aquifer groundwater have an elevated dissolved calcium concentration. The source of the calcium is from the dissolution of limestone and/or Ca-plagioclase minerals (Walter et al. 2018, 2023; Boumaiza et al. 2022d).

3. Materials and methods

3.1 Lithofacies identification, sampling, and codification

Nine sandpits (identified as 1 to 9 in Fig. 1) were selected over the study area for sampling and analysis. These sandpits offered exposed faces, which allowed lithofacies to be visually delineated and mapped based on the structure and texture of sediments. In addition, fresh sediments were manually sampled for physical properties determination. Sampling occurred after removing the ~15 cm-layer directly exposed to sun/air. For determining properties by granulometric analysis (section 3.2), about 600 g of sediment was collected at each site from the fresh-exposed face using a sampler-spoon, which was cleaned with dry towels after each collection to minimize fluid cross-transmission, and then the samples were stored in separately labeled polyethylene bags. A total of 27 sediment samples were collected from the nine selected sandpits and transported to the laboratory of the *Université du Québec à Chicoutimi* for grain size analyses. For determining sediment properties by drying (section 3.2), samples were collected from fresh-exposed faces using a specific metal cylinder of a given volume (71 cm^3), and immediately sealed to prevent moisture loss due to evaporation. Some lithofacies dominated by coarse-grained sediments were not sampled due to the difficulty in driving the sampler-metal cylinder into the sediments. A total of 24 samples were collected for physical analysis.

The samples were codified according to two main classifications. The first approach, adapted from Zappa et al. (2006), is used to codify the coarse-grained sediments.

This codification consists of determining the dominant grain size class (>50%) for which a capital letter is used (e.g., "G" for gravel). The capital letter of the code is preceded by a lowercase letter representing the particle size fraction of the dominant grain size class, for which "f" is employed for a fine fraction, whereas "c" is used for a coarse fraction. A third lowercase letter, placed at the end of lithofacies code, is used to describe the sediment structure (e.g., "h" for horizontal stratification). If two comparable grain size classes dominate a given lithofacies, the relative code then combines these two dominants' classes, e.g., "SG" for a lithofacies consisting of sandy gravel. If a grain size class is dominated (e.g., 70% of sand) with a second class having 10-30% material (e.g., 25% of gravel), the corresponding code then includes the dominant class with a capital letter and second class with a lowercase letter (e.g., fSgh code corresponds to fine sand with 10-30% of gravel material having horizontal stratification). The second coding approach, proposed by Miall (1978), is used to codify fine-grained sediments, such as clay lithofacies. For this group, specific codes are used. For example, Fm corresponds to fine-grained sediment constituted of massive clay.

3.2 Measurement of hydrogeological properties of lithofacies

Measurements of porosity and hydraulic conductivity of unlithified sediments contain variable degrees of error based on field and laboratory conditions. Such aspects as the size of a sample, and whether it is truly representative of the lithofacies in which it occurs are judgement based. Therefore, all of the measurements are actually estimates made using the best available methods and using due care during the measurement process. Careful statistical analysis ends in constricting the impacts of the error range of individual

measurements and is useful in aiding characterization of heterogeneous granular aquifers, particularly for modeling of groundwater flow and solute transport.

3.2.1 Porosity

3.2.1.1 Laboratory measurement of the porosity

After measuring the total weight (g) of the sediment samples stored in metal cylinders, they were placed in an oven for 48h at a temperature of 105 °C, and the dry sediment weights (g) were then determined. The dry bulk density (D_b, g/cm^3) was determined using Eq. 1, and used to calculate n for each sediment sample using Eq. 2 (Black et al. 1965). Here, a particle density (ρ_p) of 2.69 g/cm^3 was assumed as lower bulk densities are not expected due to the absence of organic matter within the vadose zone of the studied sandpits (Boumaiza et al. 2015, 2017, 2019).

$$D_b = \frac{\text{weight of dry soil}}{\text{volume of specific cylinder}} \quad (1)$$

$$n = 100 \cdot \left[1 - \left(\frac{D_b}{\rho_p}\right)\right] \quad (2)$$

3.2.2.1 In-situ measurement of the porosity

A porosimeter was developed at the *Université du Québec à Chicoutimi* for an in-situ measurement of n. This porosimeter (Fig. 2) consists of a sampler-cylindrical tube measuring 20.4 cm in length with 10.14 cm in diameter. The cylindrical tube is sealed at one extremity whereas its other end is open with a bevelled-boundary allowing its insertion with limited disturbance of the sampled sediments. The sampler-cylindrical tube is connected to a graduated small water-supply container by a flexible plastic pipe, which is

equipped with a control-valve with a connection to the cylindrical tube at an injection point located at its base. In the field, the sampler-cylindrical tube was used to collect full cylindrical samples from the sandpit fresh-exposed face. When this cylindrical sediment sample is collected, it is maintained vertically and connected to the water-supply container, which is maintained higher than the cylindrical tube by using a solid-support (Fig. 2). The base-location of the water injection point ensures an upward evacuation of the air within the cylindrical sample, therefore, providing a relatively complete filling of the sediment sample voids by the injected water. As soon as the first traces of water appear on the top surface of the cylindrical sediment sample, the water injection rate is reduced, using the control-valve, until the complete saturation of the sample; the control-valve is then totally closed.

Using the porosimeter, n was measured based on Eq. 3 with pore volume representing the volume of the injected water (cm^3), while the total volume is the volume of the sampler-cylindrical tube (1647 cm^3). However, it was necessary to consider the initial volumetric water content (θ_V) of the collected sediment samples. The in-situ n was then calculated by summing θ_V and n from porosimeter-based method, therefore expressing porosity in %. The collected metal cylinder samples, used to measure n in laboratory, were simultaneously used to evaluate θ_V. The gravimetric water content (θ_G) of each single sediment sample (expressed in %) was firstly determined according to Eq. 4 with all units in g (Gardner 1965). Once θ_G was estimated, the θ_V (expressed in %) was assessed using Eq. 5 (Gardner 1965), assuming a water density (ρ_w) of 1 g/cm^3. To maintain the same sampling conditions, the distance between the sampling point of the porosimeter-cylindrical tube and that of the metal cylinder did not exceed 30 cm.

$$n = \frac{\text{volume of voids}}{\text{total volume}} \quad (3)$$

$$\boldsymbol{\theta_G} = \frac{\text{weight of wet soil} - \text{weight of dry soil}}{\text{weight of dry soil}} \cdot 100 \quad (4)$$

$$\boldsymbol{\theta_V} = \theta_G \cdot \frac{\boldsymbol{D_b}}{\boldsymbol{\rho_w}} \quad (5)$$

3.2.2 Hydraulic conductivity

3.2.2.1 Laboratory measurement of the hydraulic conductivity

The present study focuses on assessing the saturated hydraulic conductivity. The sediment samples collected in separately labeled polyethylene bags were subjected to granulometric analyses for generating representative grain size curves (% passing versus grain diameter), which were used to predict *K*. In the present study, grain size sieve analysis was performed on the coarse-grained sediment samples, whereas the fine-grained sediment samples were analyzed by a hydrometer, following the procedure described by Robitaille and Tremblay (1997). The Wentworth classification is used to distinguish the sediments (clay: <0.003 mm, silt: 0.003-0.06 mm, fine sand: 0.06-0.5 mm, coarse sand: 0.5-2 mm, fine gravel: 2-4 mm, coarse gravel: 4-64 mm, pebbles: >64 mm) (Wentworth 1922). Several grain diameter-based predictive equations for *K* have been proposed (Masch and Denny 1996; Chapuis 2012). In this study, five empirical equations are selected to evaluate *K*: Hazen (1892), Beyer (1964), Chapuis (2004), Sauerbrey (1932), and USBR (Vukovic and Soro 1992). These five selected empirical equations, with their characteristics and applicable conditions, are summarized in Table 1. They are selected to consider a wide range of applicability conditions. Nonetheless, each sediment sample is finally represented by a single mean *K* value from the applied empirical equations.

Table 1. Selected empirical equations used to predict K and the applicability conditions.

Method	Empirical formula	Conditions
Hazen	K (cm/s) = $(d_{10})^2$ with d_{10} in mm	a. Sand and gravel b. $C_u \leq 5$ c. 0.1 mm $\leq d_{10} \leq$ 3 mm
Chapuis	K (cm/s) = $2.4622((d_{10})^2 e^3)/(1+e))^{0.7825}$ with d_{10} in mm	a. All natural sediments b. 0.003 mm $\leq d_{10} \leq$ 3 mm c. $0.3 \leq e \leq 1$
Beyer	K (cm/s) = $0.45(d_{10})^2 \log(500/C_u)$ with d_{10} in mm	a. Sand b. 0.06 mm $\leq d_{10} \leq$ 0.6 mm c. $1 \leq C_u \leq 20$
Sauerbrey	K (cm/s) = $2.436 n^3 (d_{17})^2/(1-n)^2$ with d_{17} in mm	a. Sand and silty sand b. $d_{10} \leq 0.5$ mm
USBR	K (cm/s) = $0.36(d_{20})^{2.3}$ with d_{20} in mm	a. Sand and gravel b. $C_u \leq 5$

d_x: effective grain size (% by weight of soil)
e: void's ratio calculated as n/1-n with n from laboratory estimation.
C_u: coefficient of uniformity of sediments ($C_u = d_{10}/d_{60}$)

3.2.2.2 In-situ measurement of the hydraulic conductivity

Several instruments have been developed for in-situ measurement of K in granular sediments (Chossat 2005). In the present study, a mini-disc infiltrometer (DDI 2012), based on the principle of infiltrated water rate into the subsurface, was used to assess K. The mini-disc infiltrometer was chosen for field measurements because it can be applied to granular sediments with less mobilization, requiring a reasonable field-operating amount of water. More details on this instrument and the relative analytical equations used for calculating K are available in (Zhang 1997; Boumaiza 2008; Naik et al. 2019).

3.2.3 Statistical analyses of sediment properties

3.2.3.1 Sediment hydraulic conductivity and porosity

Statistical correlation between the in-situ estimations and those assessed in laboratory, both for n and K, were conducted. First, the distribution of the investigated hydrogeological properties was evaluated using a Gaussian kernel density plot (Duong 2007), which is a smoother-based data visualization technique to assess the distribution of samples. Usually, the plot x-axis considers the data set variation, while the y-axis of a density plot represents

the probability density. The kernel density plot is an effective technique as it is a non-parametric way to analyze the distribution of a set of variables (Petrelli 2021). Second, the normality of the distribution was evaluated by using the Shapiro-Wilk test (Shapiro and Wilk 1965), which states a null hypothesis that the set variables are normally distributed. If the test *p*-value is <0.05 (confidence level), then the null hypothesis is rejected, and the distribution is considered not normal. Otherwise, if the *p*-value >0.05, the null hypothesis is not rejected, and the analyzed dataset with variable distribution is statistically normal. A third statistical tool was used to evaluate the trend tendency of the investigated hydrogeological properties via the Mann-Kendall test (Mann 1945; Kendall 1975) integrated into the XLSTAT software (Addinsoft 2021). A positive Kendall τ value corresponds to an upward trend, whereas a negative Kendall τ value indicates a downward trend. Note that an associated Kendall test *p*-value <0.05 denotes a significant trend, whereas a *p*-value >0.05 indicates no significant trend tendency (Pohlert 2020).

3.2.3.2 Sediment grain size Folk parameters

Sediment grain size analysis was based on the statistical parameters of Folk and Ward (1957) by using the cumulative grain size frequencies versus the grain diameter of the analyzed sediment samples. Four grain size statistical parameters were used, including the mean grain diameter (M, Eq. 6), the sorting (σ, Eq. 7), the skewness (S_k, Eq. 8), and the kurtosis (K_u, Eq. 9), all expressed in Φ_x units, which represents the $-\log_2$ grain diameter [mm] corresponding to the x-cumulative frequency (Krumbein 1934). The Folk classifications were used to distinguish σ, S_k, and K_u sediment parameters (Folk 1980). The σ values were classified as follows: σ <0.35 very well sorted, σ = 0.35-0.5 well sorted, σ = 0.5-0.71 well moderately sorted, σ = 0.71-1 moderately sorted, σ = 1-2 poorly sorted, σ =

2-4 very poorly sorted, σ >4 extremely poorly sorted. The S_k values were classified as follows: S_k = −1 to −0.3 very fine skewed, S_k = −0.3 to −0.1 fine skewed, S_k = −0.1 to +0.1 symmetrical, S_k = +0.1 to +0.3 coarse skewed, S_k = +0.3 to +1 very coarse skewed. The K_u values were classified as follows: K_u <0.6 very platykurtic (very flat), K_u = 0.67-0.9 platykurtic (flat), K_u = 0.9-1.11 mesokurtic (not especially peaked), K_u = 1.11-1.5 leptokurtic (highly peaked), K_u = 1.5-3 very leptokurtic (very highly peaked), K_u >3 extremely leptokurtic (extremely highly peaked).

$$M = \frac{\Phi_{16} + \Phi_{50} + \Phi_{84}}{3} \tag{6}$$

$$\sigma = \frac{\Phi_{84} - \Phi_{16}}{4} + \frac{\Phi_{95} - \Phi_{5}}{6.6} \tag{7}$$

$$S_{\mathrm{k}} = \frac{\Phi_{84} + \Phi_{16} - 2\Phi_{50}}{2\,(\Phi_{84} - \Phi_{16})} + \frac{\Phi_{5} + \Phi_{95} - 2\Phi_{50}}{2\,(\Phi_{95} - \Phi_{5})} \tag{8}$$

$$K_{\mathrm{u}} = \frac{\Phi_{95} - \Phi_{5}}{2.44\,(\Phi_{75} - \Phi_{25})} \tag{9}$$

4. Results

4.1 Defined and described lithofacies

A total of 27 lithofacies were identified in the study area. Within the sandpits, diverse lithofacies were commonly observed on the same investigated face (see example on Fig. 3), with some lithofacies observed at more than one stratigraphic position and identified in several distinct sandpits. Lithofacies diversity in the studied paleodeltaic system is expressed by their texture, where the corresponding grain size distribution curves of the identified lithofacies showed textures including pebbles, gravel, sand, silt and clay (Fig. 4). The sediment grain size fraction varies between fine and coarse from one lithofacies to

another. Sedimentary structures also reveal the mechanism acting during deposition, which also contributes to the diversity of lithofacies types. Several different sedimentary structures were observed. For example, at sandpit #6 (Fig. 3), the pebbly-gravel lithofacies Pgp was observed with planar laminations, whereas the coarse-sandy lithofacies cSt showed trough-laminations. The identified lithofacies are described in Table 2 along with their corresponding location, observed sedimentary structure, composition material, and established code.

Table 2. Description of lithofacies identified through the selected sandpits.

Sandpit	Observed in-situ structure of sediments	% of sediment material						Lithofacies main material composition	Code
		Pebbles	Gravel		Sand		Silt & Clay		
			Coarse gravel	Fine gravel	Coarse sand	Fine sand			
#6	Laminated structure	-	-	-	-	-	100	Clay	Fsc
#9	Massive structure	-	-	-	-	-	100	Clay	Fm
#4	Ripple cross-laminations	0	0.9	2.2	27.4	50.7	15	Fine sand with fine material	fSfr
#1	Ripple cross-laminations	0	0	0.1	0.7	91.3	6.9	Fine sand	fSr
#6	Ripple cross-laminations	0	0.1	0.1	2.1	93.1	4.2	Fine sand	fSr
#1	Horizontal laminations	0	0	0.1	31.9	66.6	1.3	Fine sand	fSh1
#1	Horizontal laminations	0	0	0	0.1	93.4	6.1	Fine sand	fSh2
#2	Horizontal laminations	0	0.8	0.8	23.6	72.9	1.8	Fine sand	fSh
#6	Trough cross-laminations	0	0.3	0.3	36.5	62.2	0.4	Fine sand	fSt
#7	Trough cross laminations	0	0	0.1	26.4	69.9	3.2	Fine sand	fSt
#1	Chaotic structure	0	0	0.4	1.3	91.9	6.1	Fine sand	fSc
#4	Planar laminations	0	0.5	2.6	28.4	61.4	3.2	Fine sand	fSp
#5	Horizontal laminations	0	0.4	2.1	60.8	36.1	0.4	Coarse sand	cSh
#2	Horizontal laminations	0	0.1	0.8	56	42.8	0.3	Coarse sand	cSh
#4	Planar laminations	0	2.3	1	71.5	21.3	0	Coarse sand	cSp
#3	Planar laminations	0	0.5	2.4	72.3	24.3	0.2	Coarse sand	cSp
#6	Trough cross laminations	0	4.6	4.9	78.2	11.7	0.3	Coarse sand	cSt
#3	Trough cross laminations	0	3.9	5.7	59.9	29.6	0.7	Coarse sand	cSt
#8	Diverse inclined stratifications	0	0.7	3.8	55	39.6	0.5	Coarse sand	cSi
#7	Trough cross laminations	0	9.8	4.9	36.5	47.6	1.1	Coarse sand with gravel	cSgt
#9	Massive structure	0	12.7	11.9	69.1	5.9	0.2	Coarse sand with gravel	cSgm
#8	Diverse inclined stratifications	0	25.2	12.2	46	16	0.3	Coarse sand with gravel	cSgi
#5	Horizontal laminations	0	35.1	3.9	41.2	18.8	0.5	Sand with gravel	Sgh
#3	Trough cross laminations	0	31.9	17.8	44.1	5.9	0.2	Sandy gravel	SGt
#8	Diverse inclined stratifications	18.5	42.2	14.7	21.2	2.9	0.3	Coarse gravel with sandy pebbles	cGspi
#5	Massive structure	48.4	21.1	4.3	17.2	7.4	1.5	Pebbles with sandy gravel	Psgm
#6	Planar laminations	63.8	23.5	4.7	5.3	2.3	0.2	Pebbles with gravel	Pgp

4.2 Results of the total porosity measurements

Porosity was measured in-situ for 22 of the 27 identified lithofacies (Fig. 5). The in-situ tests were not undertaken on lithofacies #6-Fsc and #9-Fm due to their dominance by clayey sediment, making measurement of porosity very difficult. The other three untested

lithofacies were #8-cGsi, #5-Psgm and #6-Pgp; as they are constituted of coarse gravel associated with pebbles, placement of the sampler-porosimeter into the exposed face of the sandpits was not possible. Similarly, *n* was not estimated in the laboratory for the above three lithofacies due to the difficulty in implementing the sampler-metal cylinder (used to evaluate θ_V) into the exposed faces. Clayey lithofacies Fsc and Fm did not exhibit the highest porosities as expected, but their average *n* value (41%) falls into the range expected for clayey material (Freeze and Cherry 1979). The highest *n* value was not found in the same lithofacies according to the two estimation methods. The highest in-situ *n* value was 53%, which was estimated for lithofacies fSr identified at sandpit #1, whereas the highest *n* value estimated in the laboratory was 45% observed for the lithofacies cSh identified at sandpit #5 (Fig. 5). Conversely, lithofacies #3-SGt shows the lowest *n* value according to the two estimation methods, i.e., 31% estimated in-situ and 34% estimated in the laboratory (Fig. 5).

A discrepancy was observed between the in-situ *n* results and those measured in the laboratory for all the identified lithofacies, except lithofacies #3-cSt, for which both measured porosities were identical (Fig. 5). The discrepancy between the in-situ and laboratory results differs from one lithofacies to another. The largest discrepancy of 10% is noted for the lithofacies #1-fSr with measured *n* values of 53% and 43%, respectively, between the in-situ and in the laboratory methods (Fig. 5). However, approximately three-quarters of the lithofacies showed a discrepancy ≤5%, which is a positive observation on the correlation between the in-situ and laboratory measurements.

4.3 Results of the hydraulic conductivity measurements

Hydraulic conductivity was measured in-situ for 19 of the identified lithofacies, and in the laboratory for 25 lithofacies. An in-situ measurement was not completed for the lithofacies hosting gravelly material (cSgt, cSgm, cSgi, Sgh, SGt, cGsi, Psgm, Pgp) due to the absence of gravel-dimensionless coefficient values, which are needed for calculation. Laboratory measurements were not completed for lithofacies Psgm and Pgp due to the applicability limits of the empirical equations used including the considered d_{10} and C_u. Results of K measured in-situ and in laboratory are presented in Fig. 6. The reported laboratory K value for each lithofacies represents a mean value from the applied empirical equations. The highest in-situ K value is 1.16×10^{-1} cm/s measured for lithofacies #8-cSi, whereas the highest laboratory K value is 6.79×10^{-1} cm/s assessed for lithofacies #8-cGsi. The highest K values according to the in-situ/laboratory measurement did not correspond to the same lithofacies, but both occurred at the same sandpit #8. Lithofacies #6-Fsc revealed the lowest in-situ K value (1.25×10^{-4} cm/s), whereas the lowest laboratory K value (3.48×10^{-8} cm/s) was measured for lithofacies #9-Fm, both of which are fine-grained sediment samples. Similar to the finding from the study of granular deposits by Ritzi et al. (2018), both measured in-situ and laboratory K values increase synchronously with relative grain size of the identified lithofacies. Nonetheless, discrepancies were observed between the in-situ and laboratory K measurements (Fig. 6).

5. Discussion

5.1 Effectiveness of the field porosimeter measurements

The distribution of the measured porosities is shown as a kernel density plot for both in-situ and laboratory porosity values in Fig. 7. The estimated in-situ and laboratory n values were found to be normally distributed with comparable mean n values. This normal

distribution is supported by Shapiro-Wilk tests indicating p-values >0.05 for the in-situ (p-value = 0.94) and laboratory (p-value = 0.54) set values. Furthermore, a clear decrease of n values, both estimated in-situ and in laboratory, versus the increase of lithofacies grain size was observed (Fig. 5). This observation was confirmed with negative Kendall τ values of −0.55 (p-value = 0.001) and −0.32 (p-value = 0.043) for in-situ n and laboratory estimations, respectively. All these observations demonstrate the usefulness of the porosimeter developed for the present study, although discrepancies may be associated with and/or amplified due to errors (discussed hereinafter) introduced during the field tests.

The measurement of n in-situ and in-laboratory requires collecting a representative sediment sample using the sampler-cylindrical tube and small metal cylinder, respectively. The sinking of the sampler-cylindrical tube or the small metal cylinder into the sandpit face occurs progressively until the end of these cylinders is just flush with the sandpit face. If the cylinders are pushed further, the collected sediment sample would be partially compacted. Conversely, if the cylinders are not efficiently pushed-in, extra "pore" volume would remain unfilled by sediment. Here, the related uncertainty level is expected to be low as the sinking is carefully proceeded. However, it remains that sediment sampling process can influence the quality of the collected samples, contributing to the discrepancy between the estimated in-situ and laboratory n values. Also, the in-situ estimation of n is based on evaluating the volume of water injected into the sampler-cylindrical tube of the porosimeter. The volume of the injected water was measured by multiplying the section of the water-supply container by the difference in its water-height corresponding to the start and the end of the test. For example, a water-height of 7.8 cm gives an in-situ n value of 36%, whereas a water-height of 8 cm provides a value of 37%. This example shows how

inaccuracies in evaluating the water-height can influence the measured *n* value. Although a full upward evacuation of the air is assumed within the cylindrical sediment sample, as the water injecting point is placed at the base of the sampler-cylindrical tube, it is possible that the pores of the tested sediment sample are not perfectly filled by water due to possible air entrapment within the cylindrical sediment sample. In this case, uncertainties on the void volume could contribute to the discrepancies between the estimated in-situ and laboratory *n* values.

5.2 Analysis of the hydraulic conductivity measurements

Although the observed increase of *K* is not statistically significant (*p*-value = 0.32) for the in-situ *K* estimations, the increasing trend for laboratory *K* values are significant (*p*-value <0.0001) with a positive Kendall τ value of +0.71. The in-situ *K* values are normally distributed according to kernel density plot (Fig. 8), with a confirming *p*-value of 0.83 from Shapiro-Wilk test. Conversely, the laboratory *K* values are not normally distributed based on the Shapiro-Wilk test, which had a *p*-value of <0.05 (i.e., the null-hypothesis, suggesting that the distribution is similar to a normal distribution, is not accepted). However, both sets of the in-situ and laboratory *K* values revealed an identical mean of 5.23×10^{-2} cm/s (Fig. 8), although discrepancies are observed between the in-situ and laboratory *K* measurements. Here, the observed discrepancies could be related to potential measurement errors during the hydraulic tests. For example, using the mini-disc infiltrometer, the infiltrating water ratio into the subsurface is considered after having reached steady-state condition (DDI 2012). Generally, this condition was evaluated by "eye", i.e., when regular evacuation of air bubbles in the infiltrometer was observed, steady-state condition was then assumed. Even though this evaluation approach is suggested, it remains subjective.

Distinguishing the representativeness of in-situ versus laboratory estimations is beyond the scope of this study, but this topic is still under discussion in the literature (Chesnaux et al. 2011; Rosas et al. 2014; Singh and Sharma 2022). Therefore, each lithofacies was finally represented by a single K and n value, each of them represents a simple mean of the in-situ and laboratory values. The obtained mean values are used to discuss the variability of K and n below.

5.3 Variability of hydraulic conductivity and porosity based on sediment properties

The mean representative K and n values of the identified lithofacies are presented in Table 3, which also includes the Folk grain size parameters (M, σ, S_k, and K_u all expressed in Φ units) with their interpretation according to the Folk classifications (Folk 1980). Some lithofacies are provided without the Folk parameters due to the absence of information on certain sediment cumulative frequencies. Overall, the range of variation of the mean estimated K for the coarse-grained sediment samples (8.53×10^{-3} to 6.79×10^{-1} cm/s) fits with previous local estimates derived from sediment sample grain size analysis and in-situ variable head permeability tests (Chesnaux and Stumpp 2018; Boumaiza et al. 2020c; b, 2021b; Labrecque et al. 2020).

The clayey lithofacies Fsc ($K = 6.25\times10^{-5}$ cm/s) and Fm ($K = 2.01\times10^{-4}$ cm/s) revealed variable K values despite being both dominated by clayey material. This is potentially related to the laminated stratification of Fsc leading to K values lower than that of Fm by one order of magnitude. Clayey lithofacies #6-Fsc and #9-Fm were not identified in the same sandpit, suggesting that different sediment local-scale depositional processes potentially cause significant changes in sediment texture that can lead to significant variability in their K values.

Table 3. Hydrogeological properties and Folk's parameters of the identified lithofacies.

Sand -pit	**lithof.**	***K*** **(cm/s)**	***n*** **(%)**	**σ (Φ)**	**σ interp.**	***M*** **(Φ)**	***S_k*** **(Φ)**	***S_k*** **interp.**	***K_u*** **(Φ)**	***K_u*** **interp.**	**oper. lithof.**	**corr. hydrof.**	***K*** **geom. mean (cm/s)**
6	Fsc	6.25×10^{-5}	44	-	-	-	-	-	-	-	F	A	1.12×10^{-4}
9	Fm	2.01×10^{-4}	38	-	-	-	-	-	-	-			
4	fSfr	4.10×10^{-2}	42	1.51	PO	1.83	-0.15	F.S.	0.85	PL	fS	B	3.32×10^{-2} to 9.37×10^{-2}
1	fSr	3.05×10^{-2}	48	0.78	MO	2.21	-0.15	F.S.	0.98	ME			
6	fSr	3.49×10^{-2}	45	0.75	MO	2.05	-0.14	F.S.	0.74	PL			
1	fSh1	6.02×10^{-2}	42	0.82	MO	1.21	0.07	SY	0.89	PL			
1	fSh2	5.19×10^{-2}	47	0.71	MO	2.31	-0.15	F.S.	1.48	LE			
2	fSh	6.06×10^{-2}	43	0.91	MO	1.35	0.06	SY	1.01	ME			
6	fSt	4.86×10^{-2}	44	0.73	MO	1.08	0.13	C.S.	0.87	PL			
7	fSt	1.85×10^{-2}	41	0.94	MO	1.45	0.11	C.S.	0.90	PL			
1	fSc	8.53×10^{-3}	41	0.80	MO	1.85	0.18	C.S.	0.82	PL			
4	fSp	2.55×10^{-2}	40	1.14	PO	1.33	-0.03	SY	0.96	ME			
5	cSh	7.29×10^{-2}	48	0.86	MO	0.74	0.23	C.S.	1.09	ME	cS		
2	cSh	3.44×10^{-2}	38	0.98	MO	0.94	0.36	VCS	0.99	ME			
4	cSp	8.59×10^{-2}	41	1.00	MO	0.36	0.05	SY	1.48	LE			
3	cSp	9.67×10^{-2}	40	0.87	MO	0.39	0.10	SY	1.19	LE			
6	cSt	1.44×10^{-1}	45	0.93	MO	0.04	-0.25	F.S.	1.42	LE			
3	cSt	9.39×10^{-2}	40	1.14	PO	0.39	-0.04	SY	1.31	LE			
8	cSi	8.46×10^{-2}	37	1.03	PO	0.69	0.18	C.S.	1.16	LE			
7	cSgt	5.11×10^{-2}	41	-	-	0.64	-	-	-	-			
9	cSgm	3.13×10^{-1}	36	-	-	-0.48	-	-	-	-			
8	cSgi	1.37×10^{-1}	36	-	-	-	-	-	-	-			
5	Sgh	1.42×10^{-1}	38	-	-	-	-	-	-	-	G	C	3.17×10^{-1}
3	SGt	3.29×10^{-1}	33	-	-	-	-	-	-	-			
8	cGspi	6.79×10^{-1}	-	-	-	-	-	-	-	-			
5	Psgm	-	-	-	-	-	-	-	-	-	-	-	-
6	Pgp	-	-	-	-	-	-	-	-	-	-	-	-

Legend:

Lithof.: Lithofacies
interp.: interpretation
oper. lithof.: operative lithofacies
corr. hydrof.: corresponding hydrofacies
geom.: geometric
σ: Sorting
MO: Moderately sorted

M: Mean grain diameter
S_k: Skewness
F.S.: Fine skewed
SY: Symmetrical
C.S.: Coarse skewed
VCS: Very coarse skewed
K_u: Kurtosis

PL: Platykurtic (Flat)
PO: Poorly sorted
ME: Mesokurtic (not especially peaked)
LE: Leptokurtic (highly peaked)
F: Fine-grained operative-lithofacies
fS: Fine sand operative-lithofacies
cS: Coarse sand operative-lithofacies
G: Gravelly operative-lithofacies

Sandy lithofacies dominated by the fine grain size fraction (fS-lithofacies) were observed in several locations of an investigated face (e.g., fSr, fSh and fSc observed in sandpit #1), as well in various other investigated sandpit sites (e.g., #1-fSr versus #6-fSr). This diversity in fS-lithofacies is distinguished by different lithofacies structures that control the hydrogeological properties (Anderson 1989b; Heinz and Aigner 2003; Biteman et al. 2004), wherein K was observed to range from 8.53×10^{-3} to 6.06×10^{-2} cm/s, and n varied between 40 and 48% (Table 3). Interestingly, two lithofacies #1-fSc and #7-fSt revealed same n value (41%), and both are moderately sorted, platykurtic, and coarsely skewed (Table 3). However, they showed K values with a different order of magnitude ($K_{\#1\text{-fSc}} = 8.53\times10^{-3}$ cm/s versus $K_{\#7\text{-fSt}} = 1.85\times10^{-2}$ cm/s). These two lithofacies are both dominated by portion of fine sand (91.9% for #1-fSc and 69.9% for #7-fSt), but #1-fSc contained 6.1% of fine material (silt and clay) compared to #7-fSt having only 3.2% of fine material (Table 2). The lower portion of silt and clay in sample #7-fSt, associated also with 26.4% of coarse sand, allowed #7-fSt to feature high K compared to #1-fSc. A clear negative trend in K with increasing mean grain diameter (Φ) was observed in other studies of granular sediments (Lopez et al. 2015, 2020). This framework accordingly supports the low K of #1-fSc, having mean grain diameter of 1.8 Φ, when compared to K of lithofacies #7-fSt featuring a mean grain diameter of 1.4 Φ (Table 3). It is possible that sedimentary structures influence K; both #1-fSc and #7-fSt are coarse skewed, as lithofacies #1-fSc is chaotic fine sand, whereas lithofacies #7-fSt featured trough cross-laminations. Although #1-fSc and #6-fSr are both composed of comparable sediment grain sizes (Table 2) and both are moderately sorted with platykurtic grains (Table 3), they revealed different K and n values (Table 3) presumably related to the influence from observations of chaotic

structure of #1-fSc versus ripple cross-stratification of #6-fSr. The lithofacies #2-fSh and #4-fSp are composed of comparable sediment grain size portions, both are symmetrical skewed with mesokurtic grains, and featured a comparable mean grain diameter (Table 2, 3). However, these two lithofacies show different values of K and n. Poorly sorted lithofacies #4-fSp showed a measured K value (2.55×10^{-2} cm/s) lower than that of the moderately sorted lithofacies #2-fSh (6.06×10^{-2} cm/s) presumably related to difference in sorting as K decreases with poorer sorting (Beard and Weyl 1973).

Fine sandy lithofacies with ripple cross-laminations were identified in sandpits #1, #6, and #4 with respective n values of 48, 45, and 42%; and respective K values of 3.05×10^{-2}, 3.49×10^{-2}, and 4.10×10^{-2} cm/s (Table 3). Here, the same identified lithofacies revealed different K and n values from one sandpit to another, with an inverse behavior between K and n values, although having a same sediment grain size distribution. It appears that there is an influence of lithofacies texture on n and K, as lithofacies #4-fSfr contained higher portion of the fine-grained sediment fraction (silt-clay) (15%) compared to lithofacies #6-fSr and #1-fSr, which contained 4.2 and 6.9% of fines respectively (Table 2). Fine-grained sediment material like clay is known to feature high n and low K; the higher specific surface area of small size grains increases the frictional resistance of water flow and provides fine-grained sediments with low K (Freeze and Cherry 1979; Fetter 2001). This explains the contribution of 15% of silt-clay material in increasing n and decreasing K of lithofacies #4-fSfr when compared to #6-fSr and #1-fSr. Also, these three lithofacies are fine skewed, but #4-fSfr is poorly sorted compared to #6-fSr and #1-fSr, which are moderately sorted (Table 3). The observed size distribution containing sand grains and fine particles of silt and clay provided the opportunity for interstitial clogging to occur, causing slower flow, dead end

pore occurrence, and longer flow pathways. The result is a lower hydraulic conductivity for the poorly sorted lithofacies (Masch and Denny 1996; Goutaland et al. 2013).

Lithofacies #6-fSr and #1-fSr have similar grain size distribution and Folk parameters, except for kurtosis (platykurtic for #1-fSr versus mesokurtic for #6-fSr), shows that micro-texture differences can cause variability in n and K (Anderson 1989a; Fraser and Davis 1998). The sediment micro-texture influence in the present study is also evidenced through the observed variability of K and n for lithofacies fSh1 and fSh2, both identified at sandpit #1, with different K values of 6.02×10^{-2} cm/s (#1-fSh1) and 5.19×10^{-2} (#1-fSh2), as well as different n values of 42% (#1-fSh1) and 47% (#1-fSh2). These two moderately sorted lithofacies are dominated by fine sand. However, they also contain small portions of fine-grained sediment measured at 1.3% in #1-fSh1 and 6.1% in #1-fSh2 (Table 2). Accordingly, the higher portion of fine-grained sediment material in #1-fSh2, when compared to that of #1-fSh2, contributed to a decrease in K. This finding of the sediment micro-texture influence is further supported by a difference in S_k and K_u values (Table 3). Changes in grain size of the lithofacies fSh1 versus fSh2, in same sandpit #1, reflect both variable sedimentation energy and difference in grain size (Heinz et al. 2003). Such differences in micro-textures and percentage of fine sediment can cause differences in sediment packing that, in turn, can influence both K and n.

Sandy lithofacies dominated by the coarse grain size fraction (cS-lithofacies) were observed in several investigated sandpits, with various sediment structures including horizontal (h), planar (p), trough cross-lamination (t), and inclined stratification (i). The two cSh lithofacies, identified in sandpits #2 and #5, exhibited variable K and n values (Table 3), despite being both moderately sorted with mesokurtic grains and being observed

in the field with similar horizontal stratification. The K of these two lithofacies is on the same order of magnitude, but the K of #2-cSh (3.44×10^{-2} cm/s) is slightly lower than that of #5-cSh (7.29×10^{-2} cm/s). As K is inversely correlated to mean grain diameter (Lopez et al. 2020), the difference in K can be related to the identified difference in the mean grain diameter. Lithofacies #2-cSh featured a mean grain diameter of 0.94 Φ, which exhibited a low K value when compared to #5-cSh which has a mean grain diameter of 0.74 Φ. Porosity of lithofacies #2-cSh (38%) is lower than that of #5-cSh (48%), despite both lithofacies being moderately sorted with comparable content of silt-clay sediment (0.3-0.4%). These observations lead to the conclusion that the difference in fine/coarse sand content within lithofacies #2-cSh and #5-cSh (Table 2), combined with the identified difference in grain skewness, could constitute the reasons why there is a difference in n between these lithofacies. The effect of sediment texture is also a possible explanation of the differences in K and n in lithofacies #3-cSt and #6-cSt. Lithofacies #3-cSt showed a lower n value (40%) when compared to #6-cSt (45%), possibly due to the grain sorting effect, as #3-cSt is poorly sorted whereas #6-cSt is moderately sorted. Also, #3-cSt and #6-cSt revealed comparable K_u values, and comparable distributions of grain sizes, but #3-cSt is symmetrically skewed while #6-cSt is fine skewed. The difference in grain skewness could contribute to the observed difference in n. Lithofacies #3-cSt features K value (9.39×10^{-2} cm/s) lower than that of #6-cSt (1.44×10^{-1} cm/s) due to the potential effect of the mean grain diameter, as #3-cSt featured mean grain diameter (0.39 Φ) greater than that of #6-cSt (0.04 Φ). Lithofacies #3-cSp and #4-cSp are both moderately sorted and symmetrically skewed with a leptokurtic classification (Table 3). They also exhibited comparable mean grain diameters and similar grain size distributions (Tables 2 and 3). All these features

provided #3-cSp and #4-cSp with comparable *K* and *n* values. Based on the grain size characteristics and moderate to small differences in sediment texture, the observed variation in *K* and *n* can be explained by difference in sediment packed caused by the textural variations.

Lithofacies identified with coarse sand containing 10-30% of gravel (cSg) were observed in the investigated sandpits #7, #8, and #9, with trough cross-laminations (#7-cSgt), inclined stratifications (#8-cSgi), and massive structure (#9-cSgm). Lithofacies #8-cSgi has a measured *K* value (1.37×10^{-1} cm/s) slightly lower than that of #9-cSgm (3.13×10^{-1} cm/s), but they have same *n* value of 36%. Based on the sediment grain size distribution, as less information on the Folk parameters are available for these lithofacies, #8-cSgi and #9-cSgm are composed of similar sediment grain size distribution providing them to have the same *n* and a slightly different *K,* probably due to the structure of the sediment caused by different current regimes during deposition (Table 2). Lithofacies #7-cSgt has measured *K* value (5.11×10^{-2} cm/s) lower by one order of magnitude than that of #9-cSgm (3.13×10^{-1} cm/s). In addition to the potential effect of sedimentary structures, the identified variability in *K* is likely caused by differences in mean grain diameter between #7-cSgm (0.64 Φ) and #9-cSgm (−0.48 Φ). Also, the fine-grained sediment portion in #7-cSgt (1.1%) is not enough to exert a noteworthy effect on *K*, but it also contributes to the difference in *K* in that the fine-grained sediment portion within #9-cSgm is only 0.2%. Variability in the investigated *K* and *n* is also observed through the gravelly lithofacies #8-cGspi and #3-SGt, wherein #8-cGspi contained 56.9% of gravel associated with 24.1% of sand and 18.5% of pebbles compared to #3-SGt which constitutes of only sand and gravel with equal portions of 50% each. Lithofacies with such a heterometric distribution, from

sand to gravel, were found to experience lower K in glaciofluvial deposits (Goutaland et al. 2013). However, both #8-cGspi and #3-SGt in the present study showed high K values of 6.79×10^{-1} cm/s and 3.29×10^{-1} cm/s, respectively, due potentially to the quasi-absence of a fine-grained sediment fraction (0.2-0.3%) (Heinz and Aigner 2003).

5.4 Corresponding hydrofacies

A hydrofacies is defined as a sedimentary medium in which the hydrogeological properties are controlled by sediment texture and structure (Klingbeil et al. 1999; Eaton 2006; Roy et al. 2006). Zappa et al. (2006) have grouped lithofacies with similar texture into operative-lithofacies (e.g., fS-operative-lithofacies) that share common characteristics. Each operative-lithofacies is defined by a range of hydrogeological properties from the corresponding grouped lithofacies. Determining hydrofacies consists of grouping a set of operative-lithofacies featuring similar ranges of variability in hydrogeological properties. Therefore, a hydrofacies is considered to be a representative elementary volume, which is constrained by its interval of variability in hydrogeological properties (Anderson 1989b; Bayer et al. 2011). In the present study, a simplified scheme of operative-lithofacies was developed by assigning four groups: (1) F-operative-lithofacies grouping fine-grained sediment samples, (2) fS-operative-lithofacies featuring fine sand, (3) cS-operative-lithofacies dominated by coarse sand, and (4) G-operative-lithofacies containing gravel and coarse-grained sediment (Table 3). Lithofacies #5-Psgm and #6-Pgp were not considered as they do not host estimations of hydrogeological properties. Within each operative-lithofacies, the values of K and n of the corresponding lithofacies are separately presented in a box-and-whisker diagram (boxplot). The boxplots consider the interquartile properties including the statistical upper quartile (Q3 50–75% above the median) and the lower

quartile (Q1 the lowest 25% of numbers), the maximum (elevated), the minimum (lower), and the geometric mean, which provide a reliable mean approximation for a wide range of values (Zappa et al. 2006; Atkinson et al. 2014).

The boxplot distributions of *K* and *n* within the determined operative-lithofacies is shown in Fig. 9. A distinguished *K*-variability interval for each operative-lithofacies is clearly observed when considering the interquartile statistical properties, including the geometric mean (Fig. 9a). Similarly, specific *n*-variability interval is distinguished for each operative-lithofacies (Fig. 9b). However, the *n*-variability of F-operative-lithofacies overlaps with *n*-variability interval of sandy operative-lithofacies fS and cS. In this case, associating F-operative-lithofacies to fS/cS-operative-lithofacies is confusing as *n*-variability intervals of these operative-lithofacies do not fit with those of *K*-variability intervals (Fig. 9). Hence, simultaneous consideration of *K* and *n* variability intervals for determining hydrofacies is not effective. Therefore, the approach followed in the present study consists of only considering *K*-variability intervals.

The F-operative-lithofacies is constrained by interquartile *K* values ranging from 9.72×10^{-5} to 1.67×10^{-4} cm/s including the geometric mean of 1.12×10^{-4} cm/s. The *K*-variability interval of F-operative-lithofacies, resulting from *K* of two lithofacies Fsc and Fm, differs from those of all the other operative-lithofacies by specific order of magnitude, providing F-operative-lithofacies with direct correspondence to particular hydrofacies featuring very low *K* (hydrofacies A).

The fS- and cS-operative-lithofacies revealed different distinct *K*-variability intervals (Fig. 9a). The fS-interquartile ranging from 2.67×10^{-2} to 5.11×10^{-2} cm/s was obtained from ten fS-associated lithofacies, while the cS-interquartile, revealing values from 7.58×10^{-2} to 1.27×10^{-1} cm/s, was obtained from ten cS-based lithofacies (Table 3). Despite different *K*-variability intervals of fS- and cS-operative-lithofacies, they are characterized by geometric means of the same order of magnitude ($K_{\text{-fS}} = 3.32\times10^{-2}$ cm/s; $K_{\text{-cS}} = 9.37\times10^{-2}$ cm/s), allowing them to correspond to same hydrofacies considered here as hydrofacies B. Finally, the G-operative-lithofacies is distinguished by interquartile *K* values of one order of magnitude ranging from 2.36×10^{-1} to 5.04×10^{-1} cm/s, with a geometric mean value of 3.17×10^{-1} cm/s. This particular range of high *K* provided G-operative-lithofacies with direct correspondence to a particular hydrofacies, named here as hydrofacies C, resulting from a set of the three lithofacies Sgh, SGt, and cGspi. The determined hydrofacies with their properties are presented in Table 3. It is noteworthy that hydrofacies could be assigned on the basis of different *K*-orders of magnitude (Ouellon et al. 2008; Bayer et al. 2011), but small ranges of *K*-variability of one order of magnitude as undertaken in the present study and other similar studies (Heinz et al. 2003; Fleckenstein and Fogg 2008) would be more suitable for accurately illustrating the deposit heterogeneities, which are present in most aquifers at various spatial scales (De Marsily et al. 2005).

In the present study, hydrofacies are determined based on a limited number of investigated sandpits. Therefore, some potential missing detail on *K*-heterogeneity over the entire study area occurs by the simple definition of only three distinct hydrofacies. However, having too many hydrofacies can lead to significant overlap of *K*-variability

intervals that subsequently leads to confused/complicated correspondence between lithofacies and hydrofacies. Also, hydrofacies A and C are defined by single geometric mean values corresponding to very low and very high *K*, whereas hydrofacies B is defined by range of variation constrained by two resulted "intermediate" geometric mean values. This necessitates a judgment on the *K* range of the hydrofacies applied to the studied aquifer, which may not be applicable to other aquifer types or geographic locations. The overall effect of anisotropy was not investigated assuming that the hydrofacies constitute a homogenous representative elementary volume, but not necessarily isotropic (Anderson 1989b).

5.5 Microscopic and bed-scale tortuosity in heterogeneous granular aquifers

The combined hydrofacies properties at the bed-scale and the variability with similar lithofacies helps define different scales of tortuosity that is important for assessing solute transport in this type of aquifer. Horizontal flow of water through the aquifer is likely controlled by the higher *K* hydrofacies and may avoid the lower *K* hydrofacies by deviating around them, thereby slowing movement of a solute but still allowing overall faster down-gradient movement compared to solute assessment using a mean aquifer value. The definition of real hydrofacies and associated lithofacies within a granular aquifer is quite significant in terms of the modeling approach taken to assess various types of solutes and how to design sensitivity analyses to assess potential transport rates. The hydrofacies within a heterogeneously siliciclastic aquifer also affect key large-scale aquifer properties including longitudinal and transverse dispersivity. Within the finer-grained lithofacies that have low hydraulic conductivity, Fickian diffusion rates would be influenced with regard to solute movement and release into the larger scale groundwater flow.

6. Conclusion

The present study reveals that deltaic granular deposits feature a great diversity in lithofacies ranging from those dominated by fine-grained sediments to those featuring coarse-grained sediments. Note that various lithofacies were often observed on the same investigated face, while others were observed in more than one stratigraphic position of an investigated face and identified at several distinct sandpits. Use of direct and indirect measurements of n and K in sandpits is shown to offer an opportunity to directly identify lithofacies and ultimately, hydrofacies within their actual structure and to define their hydraulic properties. This type of investigation allows a more comprehensive assessment to be made on the actual degree of aquifer heterogeneity and how it can be applied to groundwater solute transport modeling.

Assessing K and n for coarse sediments, particularly pebbly gravel lithofacies, is still challenging and will require developing new measurement tools beyond those used in the present study. Improvement of the approach to the measurement of the coarse-grained lithofacies types could further improve aquifer characterization. However, coarse-grained lithofacies commonly contain poor sorting and may not increase the magnitude of the K values in hydrofacies. The present study highlights the usefulness of the developed porosimeter utilized for in-situ evaluation of the porosity, and therefore, this porosimeter can be adopted for future studies in diverse geographic regions. However, it is limited to conducting measurements within sandy-gravelly material, as pebbly material was found to inhibit sinking the sampler-cylindrical tube of the porosimeter into the sediment, while fine-grained sediment like clay was observed to inhibit water percolation.

As expected, variability in *K* and *n* was clearly observed between the fine-grained lithofacies and those featuring coarse-grained sediments. Within the groups of operative-lithofacies, a clear impact of sediment texture and structure was observed. Several lithofacies featuring the same class and grain size fraction were observed with variable *K* and *n* caused by minor changes in textural properties. Grain size analyses were relevant to correctly designate lithofacies and their corresponding codes. Particular attention is required in the identification of lithofacies units because direct field observation in stead of sediment texture assessment can be misleading. For example, sometimes what appears to be a fine-sand lithofacies contains a coarse sand dominated grain size distribution found during laboratory grain size analysis. The influence of sedimentary structures on *K* and *n* was assessed through the results from lithofacies having similar texture but featuring differing sedimentary structures. The differing processes occurring during deposition led to minor texture variation that impacts *K* and *n* values in similar lithofacies. The Folk grain size parameters were helpful in describing the difference between lithofacies, with comparable outcomes to other studies showing that mean diameter and sorting of grains have significant effect on the variability of *K* and *n*.

This investigation clearly confirmed the degree of hydrogeological heterogeneity within deltaic systems. Correspondence of lithofacies identified in the Valin River paleodelta with different *K* and *n* values into operative-lithofacies led subsequently to determine different hydrofacies that control large-scale groundwater flow patterns. However, simultaneous consideration of *K* and *n* for determining hydrofacies was found to be inappropriate because of the overlapping values of *n*, thereby requiring solely the use of *K*. This issue does not underestimate the importance of *n*, which was found to be a relevant

property for other interpretations. Finally, this research demonstrates that even based on a limited number of investigated sandpits, the relevant basic information obtained is useful in defining the degree of aquifer heterogeneity, in developing conceptual hydrogeological models, and for evaluating groundwater flow and contaminant transport.

Figures

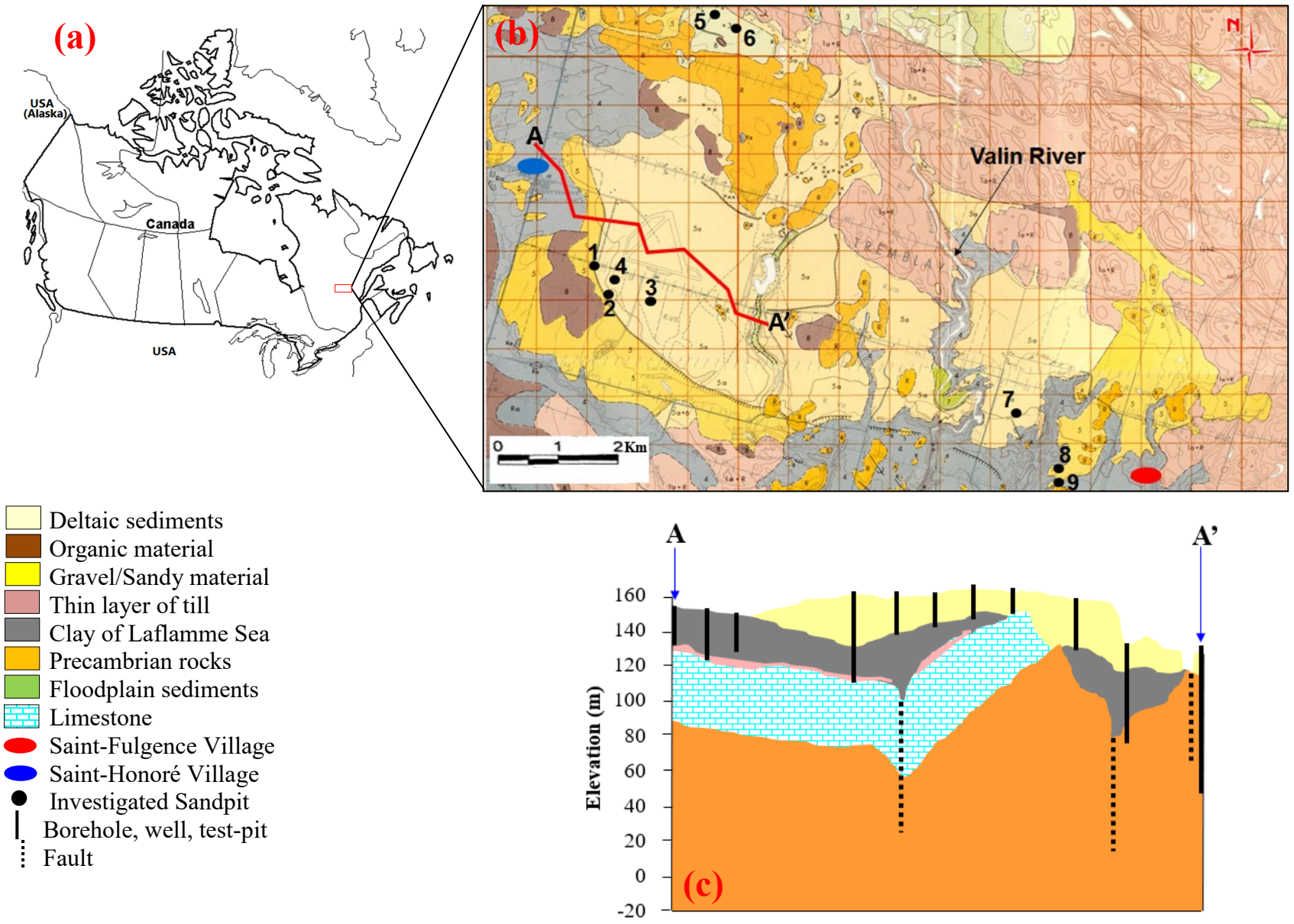

Fig. 1. (a) Geographic location of study area with (b) detail on the geology of surface deposits (Lasalle and Tremblay 1978), and (c) subsurface cross-section AA' (CERM-PACES 2013).

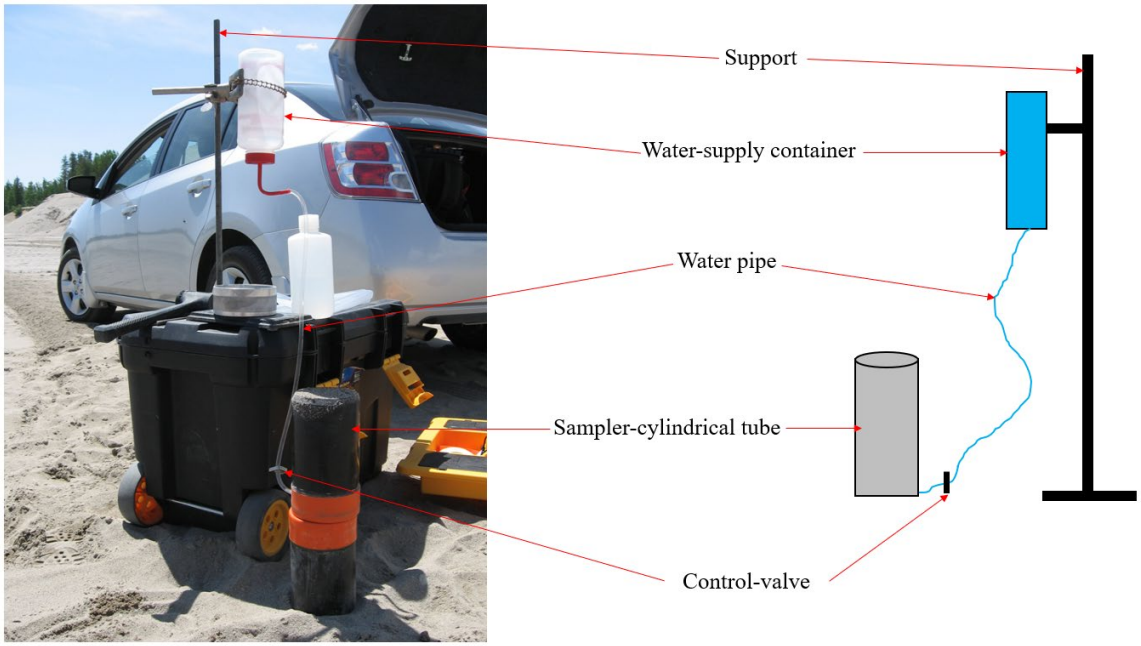

Fig. 2. Porosimeter used in this study with a general overview of its components.

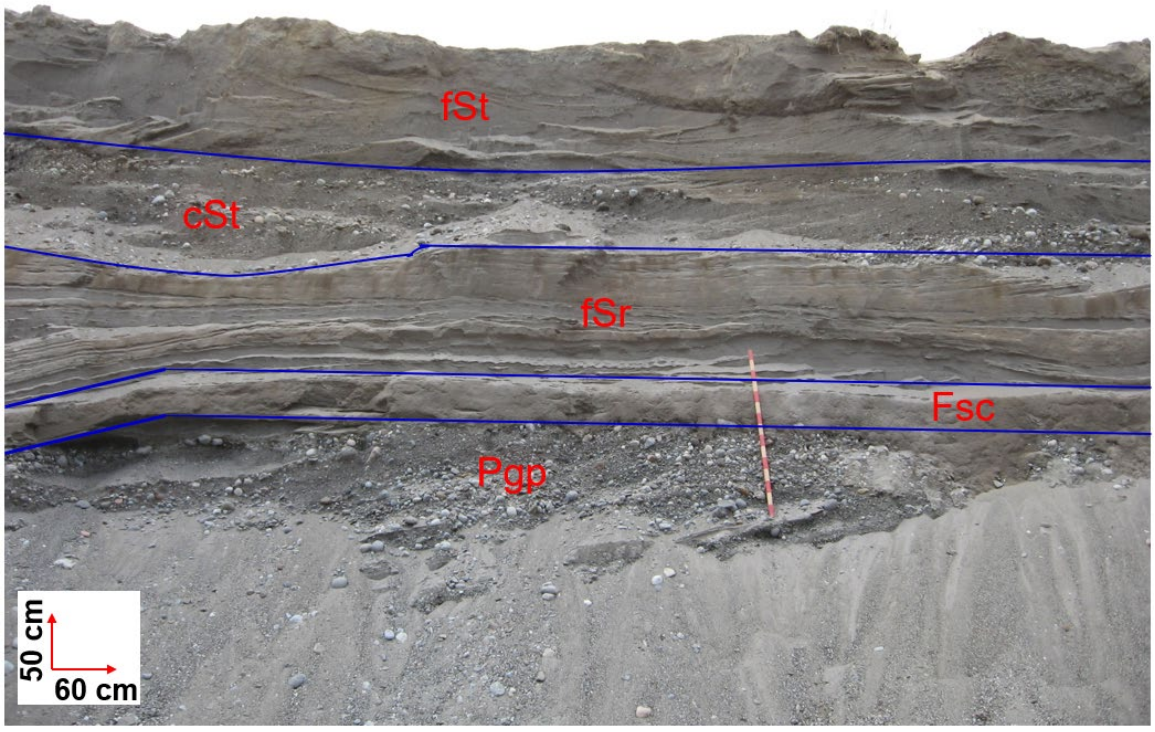

Fig. 3. Example of the identified lithofacies on the exposed face of sandpit #6.

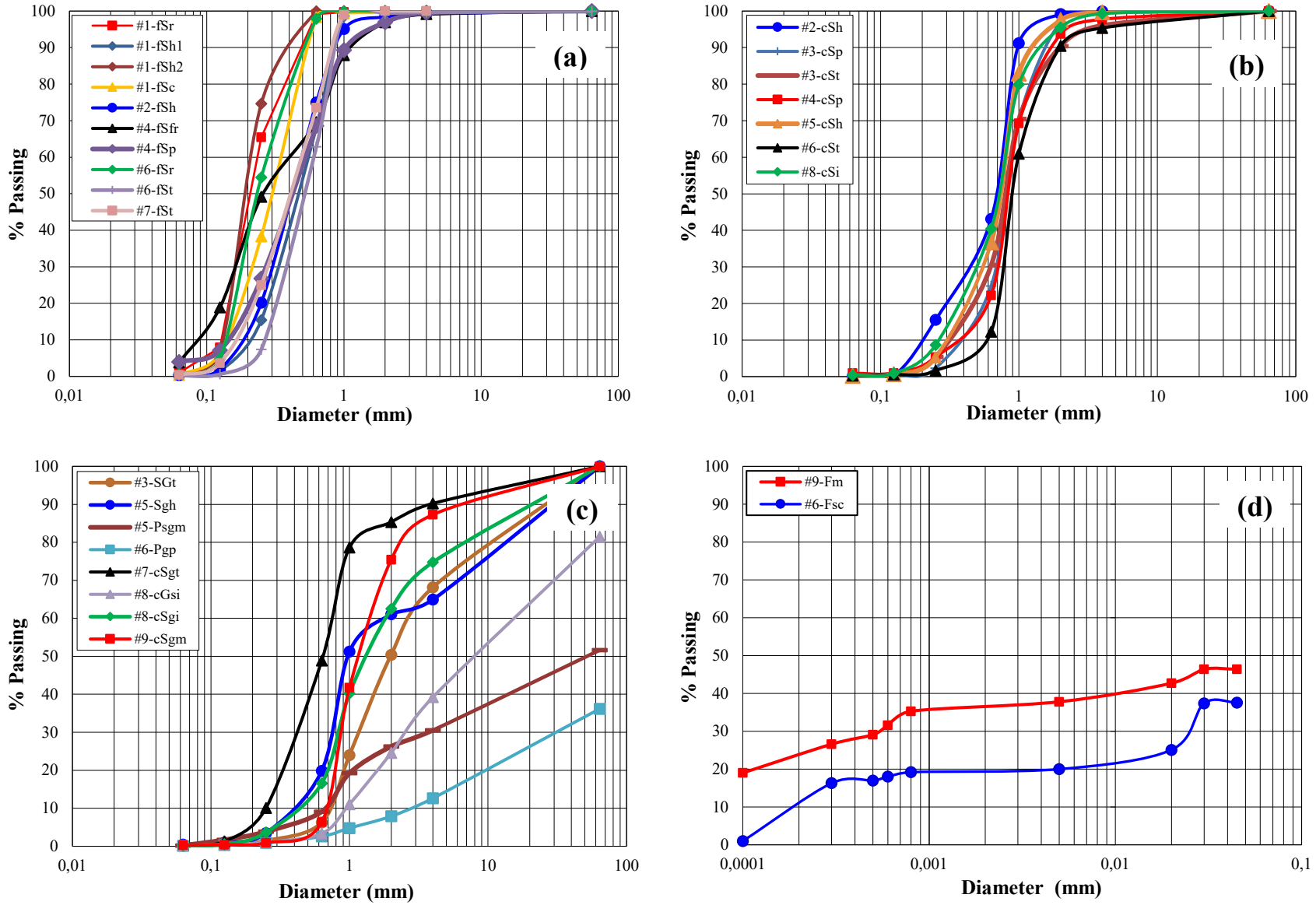

Fig. 4. Grain-passing percentages versus diameter for (a) fine-sandy sediment samples, (b) coarse-sandy sediment samples, (c) sediment samples containing considerable gravelly/pebbly fraction, and (d) fine-grained sediment samples. The codes (e.g., #1-fSr) on the figure correspond to number of sandpit (e.g., #1) with the lithofacies code (e.g., fSr).

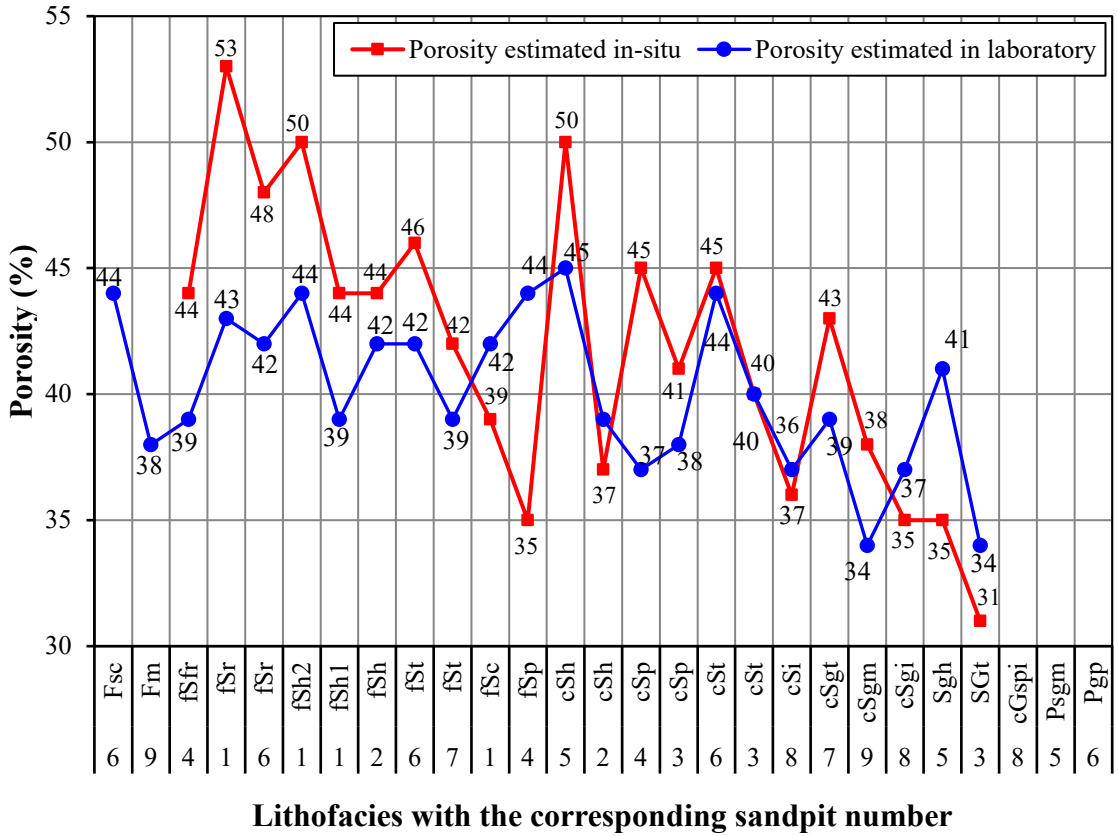

Fig. 5. Results of *n*, measured in-situ and in laboratory, of the identified lithofacies that are presented from fine (left) to coarse (right) grained-sediments. The solid lines connecting the plotted points do not signify any connection between the tested sites; they are rather introduced here to highlight potential trend.

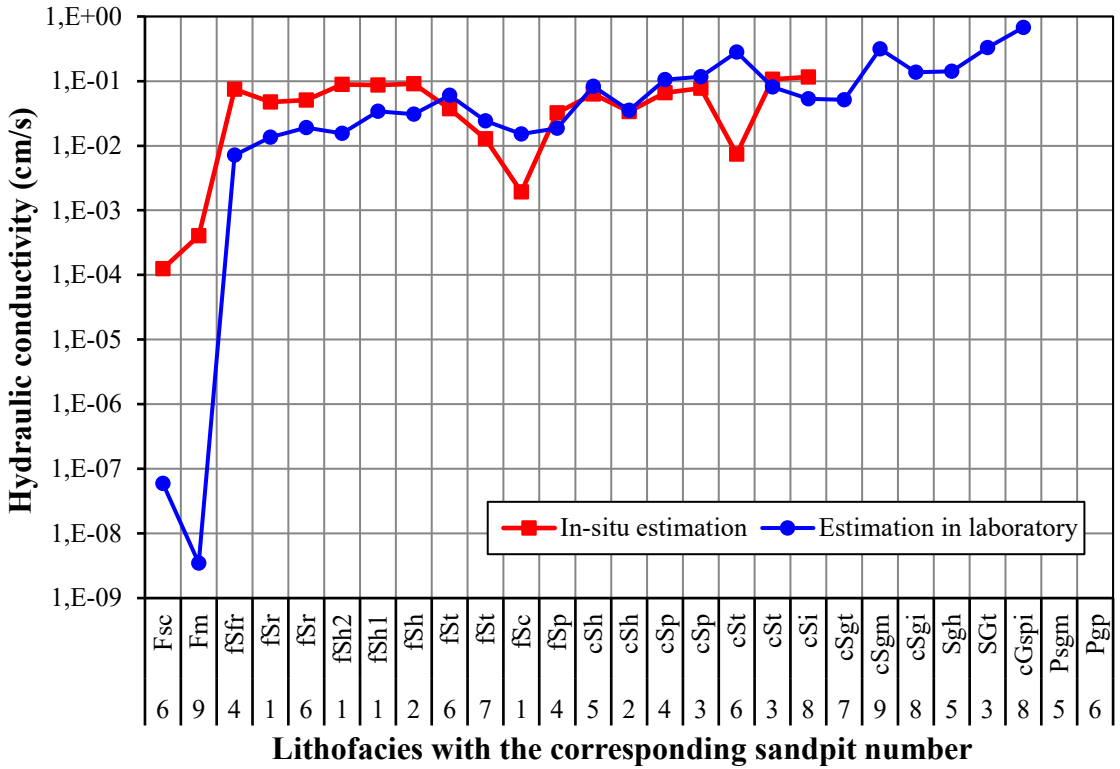

Fig. 6. Results of *K* measured in-situ and in laboratory, of the identified lithofacies that are presented from fine (left) to coarse (right) grained-sediments.

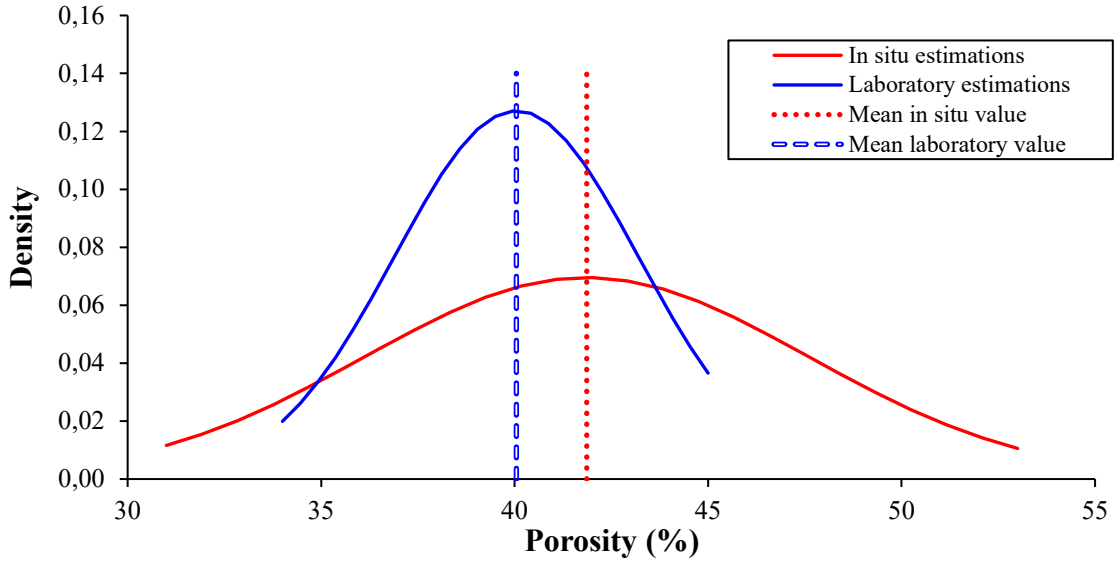

Fig. 7. Density plot showing the distribution of *n* values of both in-situ and laboratory measurements.

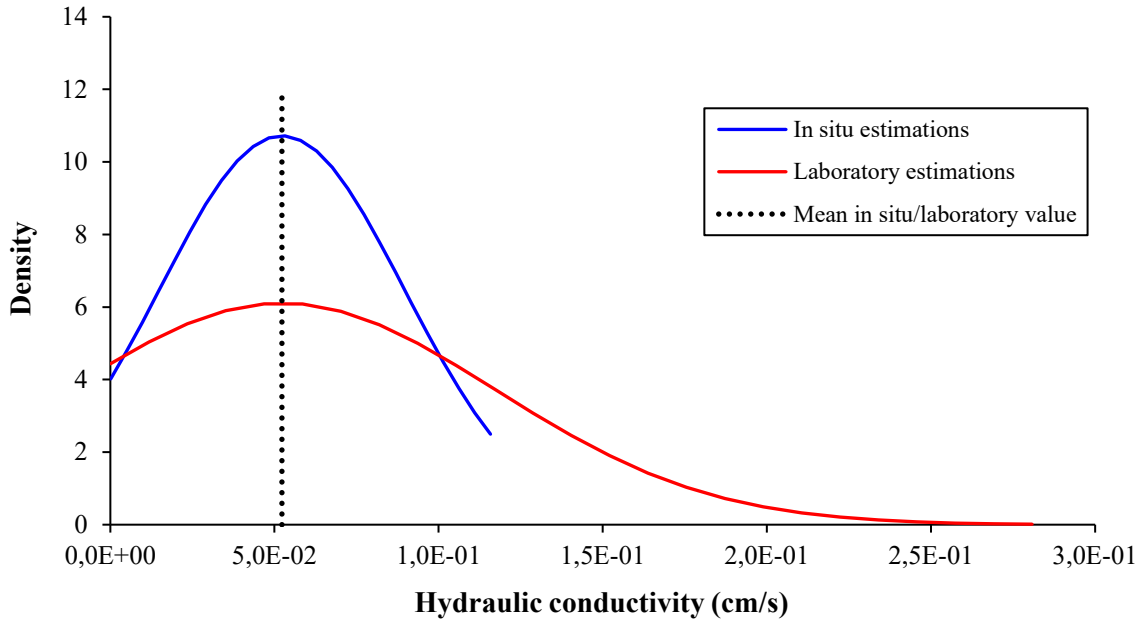

Fig. 8. Density plot illustrating the distribution of *K* values of both in-situ and laboratory estimations.

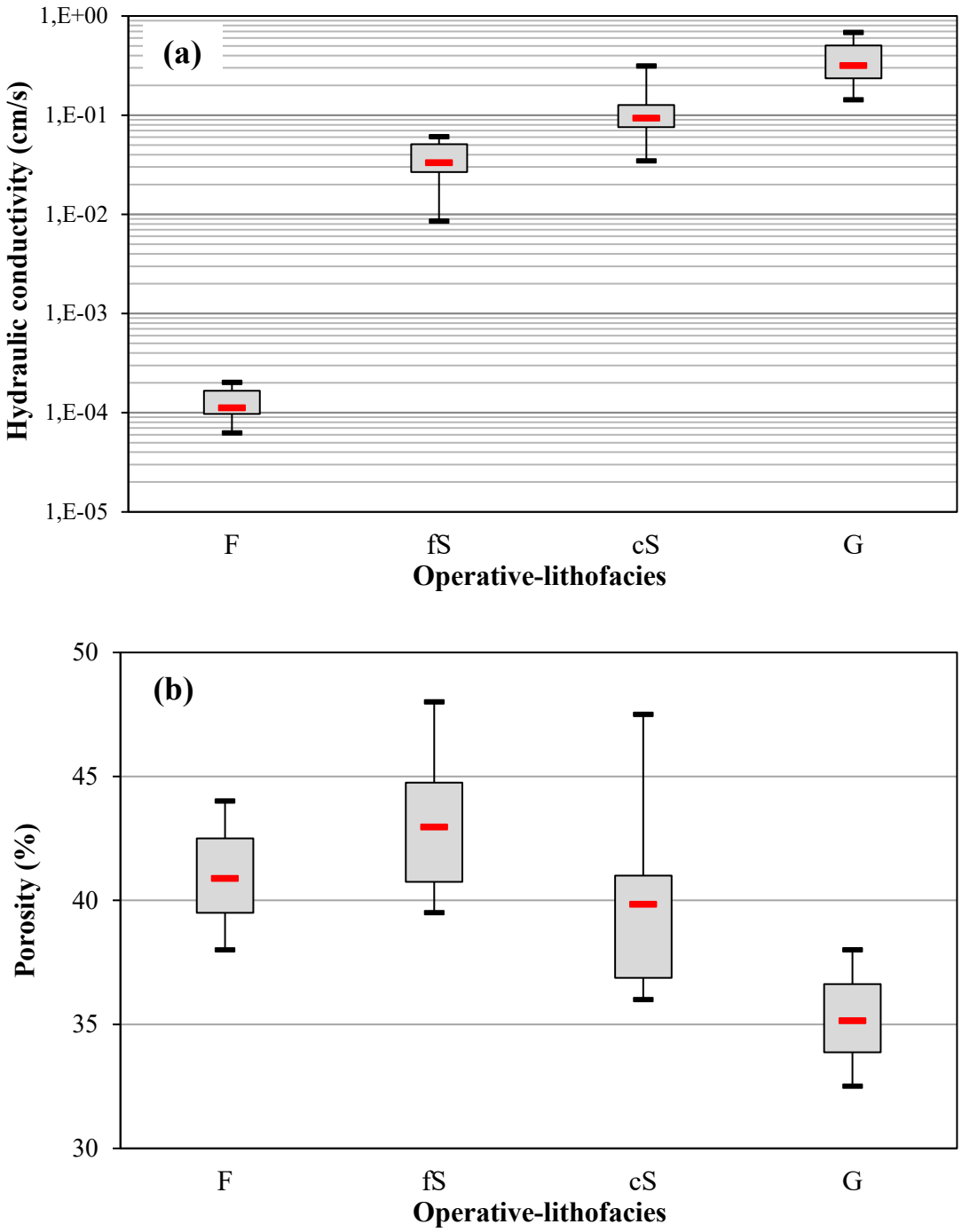

Fig. 9. Boxplot distribution of (a) *K* values and (b) *n* values for the determined operative lithofacies (F: Fine-grained-operative-lithofacies; fS: Fine sand-operative-lithofacies; cS: Coarse sand-operative-lithofacies; G: Gravelly-operative-lithofacies).

Declaration of competing interest

The authors declare that they have no known competing financial interests or personal relationships that could have appeared to influence the work reported in this paper.

Data availability

Data used for the present study are provided and described in the manuscript.

Acknowledgements

The authors thank the Natural Sciences and Engineering Research Council of Canada, which have funded this project through NSERC-Discovery Grant (RGPIN/07117) held by Prof. Romain Chesnaux. The authors also acknowledge the financial support from the *Comité de liaison institutionnel* of the *Université du Québec à Chicoutimi* (Grant number CLI-57404 held by Dr. Lamine Boumaiza). The authors would like to thank Ms. Maryse Doucet from *Université du Québec à Chicoutimi* (Quebec, Canada) for her help during fieldwork.

References

Addinsoft (2021) XLSTAT statistical and data analysis solution. New York, USA. https ://www.xlsta t.com

Amiri V, Sohrabi N, Li P, Shukla S (2022) Estimation of hydraulic conductivity and porosity of a heterogeneous porous aquifer by combining transition probability geostatistical simulation, geophysical survey, and pumping test data. Environ Dev Sustain. https://doi.org/https://doi.org/10.1007/s10668-022-02368-6

Anderson MP (1989a) Hydrogeologic facies models to delineate large-scale spatial trends in glacial and glaciofluvial sediments. Geol Soc Am Bull 101:501–511

Anderson MP (1989b) Hydrogeologic fades models to delineate large-scale spatial trends in glaciofluvial sediments. Geol Soc Am Bull 501–511

Atkinson LA, Ross M, Stumpf AJ (2014) Three-dimensional hydrofacies assemblages in ice-contact/proximal sediments forming a heterogeneous 'hybrid' hydrostratigraphic unit in central Illinois, USA. Hydrogeol J 22:1605–1624

Bayer P, Huggenberger P, Renard P, Comunian A (2011) Three-dimensional high resolution fluvio-glacial aquifer analog: Part 1: Field study. J Hydrol 405:1–9

Beard DC, Weyl PK (1973) Influence of texture on porosity and permeability on

unconsolidated sand. Am Assoc Pet Geol Bull 57:349–369
Becht A, Burger C, Kostic B, Appel E, Dietrich P (2007) High-resolution aquifer characterization using seismic cross-hole tomography: An evaluation experiment in a gravel delta. J Hydrol 336:171–185
Beyer W (1964) Zur bestimmung der wasserdurchlässigkeit von kiesen und sanden aus der kornverteilungskurve [On determining the water permeability of gravel and sand from the grain distribution curve]. Wasserwirtsch Wassertech 14:165–168
Bierkens MF., Weerts HJT (1994) Block hydraulic conductivity of cross-bedded fluvial sediments. Water Resour Res 30:2665–2678
Biteman S, Hyndman DW, Phanikumar MS, Weissmann GS (2004) Integration of sedimentologic and hydrologeologic properties for improved transport simulations. Bridge, J., Hyndman, D.W. (Eds.), Aquifer Characterization. SEPM Special Publication, n°80. SEPM Society for Sedimentary Geology, Tulsa, Oklahoma, pp 3–13
Black CA, Evans DD, White JL, Ensming LE, Clark FE, Dinaueu RC (1965) Methods of soil analysis, Part 1, Physical and mineralogical properties including staistics of measurement and sampling. American Society Agronomy, Inc Publisher. Madison. Wisconsin USA
Boumaiza L (2008) Caractérisation hydrogéologique des hydrofaciès dans le paléodelta de la rivière Valin au Saguenay [Hydrogeological characterization of hydrofacies in the Valin River Paleodelta in Saguenay]. Master's Thesis, Université du Québec à Chicoutimi, Québec, Canada
Boumaiza L, Chesnaux R, Drias T, Walter J, Huneau F, Garel E, Knoeller K, Stumpp C (2020a) Identifying groundwater degradation sources in a Mediterranean coastal area experiencing significant multi-origin stresses. Sci Total Environ 746:1–20
Boumaiza L, Chesnaux R, Walter J, Meghnefi F (2021a) Assessing response times of an alluvial aquifer experiencing seasonally variable meteorological inputs. Groundw Sustain Dev 14:1–12. https://doi.org/doi.org/10.1016/j.gsd.2021.100647
Boumaiza L, Chesnaux R, Walter J, Stumpp C (2020b) Constraining a flow model with field measurements to assess water transit time through a vadose zone. Groundwater. https://doi.org/doi.org/10.1111/gwat.13056
Boumaiza L, Chesnaux R, Walter J, Stumpp C (2020c) Assessing groundwater recharge and transpiration in a humid northern region dominated by snowmelt using vadose-zone depth profiles. Hydrogeol J 28:2315–2329
Boumaiza L, Chesnaux R, Walter J, Stumpp C (2021b) Numerical assessment of water transit-time through a thick heterogeneous aquifer vadose-zone. In: Proceedings of the 74th Canadian Geotechnical Conference and the 14th Joint CGS/IAH-CNC Groundwater Conference (GeoNiagara-2021), Niagara Falls, Ontario, Canada. p 6
Boumaiza L, Rouleau A, Cousineau PA (2015) Estimation de la conductivité hydraulique et de la porosité des lithofaciès identifiés dans les dépôts granulaires du paléodelta de la rivière Valin dans la région du Saguenay au Québec [Estimation of the hydraulic conductivity and porosity of the lithofacies identified in the granular deposits of the paleodelta of the Valin River in the Saguenay region of Quebec]. In: Proceedings of the 68th Canadian Geotechnical Conference, Quebec City, Quebec, Canada. p 9
Boumaiza L, Rouleau A, Cousineau PA (2017) Determining hydrofacies in granular deposits of the Valin River paleodelta in the Saguenay region of Quebec. In:

Proceedings of the 70th Canadian Geotechnical Conference and the 12th Joint CGS/IAH-CNC Groundwater Conference, Ottawa, Ontario, Canada. p 8

Boumaiza L, Rouleau A, Cousineau PA (2019) Combining shallow hydrogeological characterization with borehole data for determining hydrofacies in the Valin River paleodelta. In: Proceedings of the 72nd Canadian Geotechnical Conference, St-John's, Newfoundland, Canada. p 8

Boumaiza L, Walter J, Chesnaux R, Zahi F, Huneau F, Garel E, Stotler RL, Bordeleau G, Drias T, Johannesson KH, Vystavna Y, Re V, Knöller K, Stumpp C (2022a) Combined effects of seawater intrusion and nitrate contamination on groundwater in coastal agricultural areas: A case from the Plain of the El-Nil River (North-Eastern Algeria). Sci Total Environ 851:1–13

Boumaiza L, Walter J, Chesnaux R, Huneau F, Garel E, Erostate M, Johannesson KH, Vystavna Y, Bougherira N, Bordeleau G, Stotler RL, Blarasin M, Gutierrez M, Knöller K, Stumpp C (2022b) Multi-tracer approach to understand nitrate contamination and groundwater-surface water interactions in the Mediterranean coastal area of Guerbes-Senhadja, Algeria. J Contam Hydrol 251:1–16

Boumaiza L, Walter J, Chesnaux R, Lambert M, Jha MK, Wanke H, Brookfield A, Batelaan O, Galvão P, Laftouhi NE, Stumpp C (2022c) Groundwater recharge over the past 100 years: regional spatiotemporal assessment and climate change impact over the Sauguenay-Lac-Saint-Jean region, Canada. Hydrol Process 36:1–17. https://doi.org/doi.org/10.1002/hyp.14526

Boumaiza L, Walter J, Chesnaux R, Stotler RL, Wen T, Johannesson KH, Karthikeyan B, Huneau F (2022d) Chloride-salinity as indicator of the chemical composition of groundwater: empirical predictive model based on aquifers in Southern Quebec, Canada. Environ Sci Pollut Res 29:59414–59432

Brauchler R, Hu R, Vogt T, Al-Halbouni D, Heinrichs T, Ptak T, Sauter M (2010) Cross-well slug interference tests: An effective characterization method for resolving aquifer heterogeneity. J Hydrol 384:33–45

CERM-PACES (2013) Résultats du programme d'acquisition de connaissances sur les eaux souterraines de la région Saguenay-Lac-Saint-Jean [Results of the groundwater knowledge acquisition program in the Saguenay-Lac-Saint-Jean region]. Centre d'études sur les ressources minérales, Université du Québec à Chicoutimi

Chapuis RP (2012) Predicting the saturated hydraulic conductivity of soils: A review. Bull Eng Geol Environ 71:401–434

Chapuis RP (2004) Predicting the saturated hydraulic conductivity of sand and gravel using effective diameter and void ratio. Can Geotech J 41:787–795

Chesnaux R, Baudement C, Hay M (2011) Assessing and comparing the hydraulic properties of granular aquifers on three different scales. In: Proceedings of Geohydro Conference, Quebec City (Quebec), Canada. pp 1–10

Chesnaux R, Elliott AP (2011) Demonstrating evidence of hydraulic connections between granular aquifers and fractured rock aquifers. In: Proceedings of GeoHydro 2011, Joint Meeting of the Canadian Quaternary Association and the Canadian Chapter of the International Association of Hydrogeologists, August 28–31, 2011, Quebec City, Quebec, Canada. p 8

Chesnaux R, Stumpp C (2018) Advantages and challenges of using soil water isotopes to assess groundwater recharge dominated by snowmelt at a field study located in

Canada. Hydrol Sci J 63:679–695
Chossat JC (2005) La mesure de la conductivité hydraulique dans les sols, Choix des méthodes [The measurement of hydraulic conductivity in soils, Choice of methods]. Paris, France: Lavoisier
Daigneault RA, Cousineau PA, Leduc E, Beaudoin G, Milette S, Horth N, Roy DW, Lamothe M, Allard G (2011) Rapport final sur les travaux de cartographie des formations superficielles réalisés dans le territoire municipalisé du Saguenay-Lac-Saint-Jean [Final report on the mapping work of surface deposits carried out in the municipal territory of Saguenay-Lac-Saint-Jean]. Ministère des Ressources naturelles et de la Faune du Québec, Canada
DDI (Decagon Devices Inc.) (2012) Mini Disk Infiltrometer user's manual version 10. Pullman, WA
De Caro M, Perico R, Crosta GB, Frattini P, Volpi G (2020) A regional-scale conceptual and numerical groundwater flow model in fluvio-glacial sediments for the Milan Metropolitan area (Northern Italy). J Hydrol Reg Stud 29:1–18. https://doi.org/10.1016/j.ejrh.2020.100683
De Clercq T, Jardani A, Fischer P, Thanberger L, Vu TM, Pitaval D, Côme JM, Begassat P (2020) The use of electrical resistivity tomograms as a parameterization for the hydraulic characterization of a contaminated aquifer. J Hydrol 587:1–8
De Marsily G, Delay F, Gonçalvès J, Renard P, Teles V, Violette S (2005) Dealing with spatial heterogeneity. Hydrogeol J 13:61–183
Duong T (2007) ks: Kernel density estimation and kernel discriminant analysis for multivariate data in R. J Stat Softw 21:1–16
Eaton TT (2006) On the importance of geological heterogeneity for flow simulation. Sediment Geol 184:187–201
Elmeknassi M, Bouchaou L, El Mandour A, Elgettafi M, Himi M, Casas A (2022) Multiple stable isotopes and geochemical approaches to elucidate groundwater salinity and contamination in the critical coastal zone: A case from the Bou-areg and Gareb aquifers (North-Eastern Morocco). Environ Pollut 300:1–13
Fetter CW (2001) Applied Hydrogeology. 4th edn. Prentice-Hall, Inc., New Jersey
Fleckenstein JH, Fogg GE (2008) Efficient upscaling of hydraulic conductivity in heterogeneous alluvial aquifers. Hydrogeol J 16:1239–1250
Fogg GE, Zhang Y (2016) Debates-stochastic subsurface hydrology from theory to practice: a geologic perspective. Water Resour Res 12
Folk RL (1980) Petrology of sedimentary rocks. HemphilPs, University of Texas, Austin
Folk RL, Ward WC (1957) Brazos River bar: a study in the significance of grain size parameters. J Sediment Petrol 31:514–529
Franco D, Coulibaly K, Kunberger T, Kinzli KD, Arbelaez S, Missimer TM (2017) Evolution of heterogeneous mixed siliciclastic/carbonate aquifers containg metastable sediment. Groundwater 55:784–796
Fraser GS, Davis JM (1998) Hydrogeologic Models of Sedimentary Aquifers, SEPM Concepts in Hydrogeology and Environmental Geology. Tulsa, Oklahoma
Freeze RA, Cherry JA (1979) Groundwater. Prentice Hall, Englewood Cliff
Gardner WH (1965) Water content. In: Black, C.A. (Ed.), Methods of Soil Analysis. American Society of Agronomy, Inc., Madison, Wisconsin, USA. pp 82–127
Goutaland D, Winiarski T, Lassabatere L, Dubé J.S, Angulo-Jaramillo R (2013)

Sedimentary and hydraulic characterization of a heterogeneous glaciofluvial deposit: Application to the modeling of unsaturated flow. Eng Geol 166:127–139
Government of Canada (2022) Canada's national climate archive. http://www.climate.weatheroffice.ec.gc.ca/climate_normals/ [consulted in July 2019]
Hazen A (1892) Some physical properties of sand and gravel, with their special reference to their use in filtration. 24th Annu report, Boston, Massachusetts State Board Heal 34:539–556
Hébert C, Lacoste P (1998) Géologie de la région de Jonquière-Chicoutimi [Geology of the Jonquière-Chicoutimi region]. Rapport géologique no. RG 96- 08, Ministère des Ressources Naturelles du Québec, Canada
Heinz J, Aigner T (2003) Hierarchical dynamic stratigraphy in various Quaternary gravel deposits, Rhine glacier area (SW Germany): implications for hydrostratigraphy. Int J Earth Sci 92:923–938
Heinz J, Kleineidam S, Teutsch G, Aigner T (2003) Heterogeneity patterns of Quaternary glaciofluvial gravel bodies (SW-Germany): Application to hydrogeology. Sediment Geol 158:1–23
Hinnell AC, Ferr TPA, Vrugt JA, Huisman JA, Moysey S, Rings J, Kowalsky MB (2010) Improved extraction of hydrologic information from geophysical data through coupled hydrogeophysical inversion. Water Resour Res 46:
Huggenberger P, Aigner T (1999) Introduction to the special issue on aquifer-sedimentology: Problems, prespectives and modern approaches. Sediment Geol 129:179–186
Iversen BV, Van der keur P, Vosgerau H (2008) Hydrogeological relationships of sandy deposits: modeling of two-dimensional unsaturated water and pesticide transport. J Environ Qual 37:1909–1917
Kendall MG (1975) Rank Correlation Method. Charless Griffin, London
Klingbeil R, Kleineidam S, Asprion U, Aigner T, Teutsch G (1999) Relating lithofacies to hydrofacies: Outcrop-based hydrogeological characterisation of Quaternary gravel deposits. Sediment Geol 129:299–310
Kostic B, Becht A, Aigner T (2005) 3-D sedimentary architecture of a Quaternary gravel delta (SW-Germany): Implications for hydrostratigraphy. Sediment Geol 181:147–171
Krumbein WC (1934) Size frequency distribution of sediments. J Sediment Geol 4:66–77
Labrecque G, Chesnaux R, Boucher MA (2020) Water-table fluctuation method for assessing aquifer recharge: application to Canadian aquifers and comparison with other methods. Hydrogeol J 28:521–533
Lasalle P, Tremblay G (1978) Dépôts meubles du Saguenay Lac Saint-Jean [Unconsolidated deposits of Saguenay Lac Saint-Jean]. Rapport géologique n° 191, ministère des Richesses naturelles du Québec, Canada
Lévesque Y, Chesnaux R, Walter J (2023) Using geophysical data to assess groundwater levels and the accuracy of a regional numerical flow model. Hydrogeol J. https://doi.org/https://doi.org/10.1007/s10040-023-02591-z
Lévesque Y, St-Onge G, Lajeunesse P, Desiage PA, Brouard E (2020) Defining the maximum extent of the Laurentide Ice Sheet in Home Bay (eastern Arctic Canada) during the Last Glacial episode. Boreas 49:52–70
Lévesque Y, Walter J, Chesnaux R (2021) Transient Electromagnetic (TEM) Surveys as a

First Approach for Characterizing a Regional Aquifer: The Case of the Saint-Narcisse Moraine, Quebec, Canada. Geoscience 11:415–442
Lopez OM, Hegy MC, Missimer TM (2020) Statistical comparisons of grain size characteristics, hydraulic conductivity, and porosity of barchan desert dunes to coastal dunes. Aeolian Res 43:1–12
Lopez OM, Jadoon KZ, Missimer TM (2015) Relationship between grain size distribution and hydraulic conductivity of dune sands: Wadi Khulays dune field, western Saudi Arabia. Water 7:6411–6426.
Ma L, Liao H, Qian J, Zhao W, Li S (2023). Upscaling equivalent hydrofacies simulation based on borehole data generalization and transition probability geostatistics, Hydrogeology Journal, doi.org/10.1007/s10040-023-02621-w
Ma L, Deng H, Yan Y, Deng Y, Zhao W, Tan X, Qian, J (2017). Hydrofacies simulation based on transition probability geostatistics using electrical resistivity tomography and borehole data, *Hydrogeology Journal*, 30, 2117-2134.
Maizels J (1993) Lithofacies variation within sandur deposits: the role of runoff regime, flow dynamics and sediment supply characteristics. Sediment Geol 85:299–325
Mann HB (1945) Nonparametric tests against trend. Econometrica 13:245–259
Maples SR, Fogg GE, Maxwell RM (2019) Modeling managed aquifer recharge processes in a highly heterogeneous, semi-confined aquifer system. Hydrogeol J 27:2869–2888
Masch FD, Denny KJ (1996) Grain size distribution and its effect on the hydraulic conductivity of unconsolidated sands. Water Resour Res 2:665–677
Miall AD (1978) Lithofacies and vertical profil models in braided river deposits : a summary. Can Soc Pet Geol 5:597–604
Mohammed N, Celle-Jeanton H, Huneau F, Le Coustumer P, Lavastre V, Bertrand G, Charrier G, Clauzet ML (2014) Isotopic and geochemical identification f main groundwater supply sources to an alluvial aquifer, the Allier River valley (France). J Hydrol 508:181–196
Naik AP, Ghosh B, Pekkat S (2019) Estimating soil hydraulic properties using mini disk infiltrometer. ISH J Hydraul Eng 25:62–70
Nutz A, Ghienne JF, Schuster M, Dietrich P, Roquin C, Hay MB, Bouchette F, Cousineau PA (2015) Forced regressive deposits of a deglaciation sequence: Example from the Late Quaternary duccession in the Lake Sait-Jean basin (Québec, Canada). Sedimentology 62:1573–1610
Nutz A, Ghienne JF, Schuster M, Certain R, Robin N, Roquin C, Raynal O, Bouchette F, Duringer P, Cousineau PA (2013) Seismic-stratigraphic record of a deglaciation sequence: from the marine Laflamme Gulf to Lake Saint-Jean (late Quaternary, Québec, Canaga). Boreas 43:309–329
Ouellon T, Lefebvre R, Marcotte D, Boutin A, Blais V, Parent M (2008) Hydraulic conductivity heterogeneity of a local deltaic aquifer system from the kriged 3D distribution of hydrofacies from borehole logs, Valcartier, Canada. J Hydrol 351:71–86
Pagé P (1999) Les grandes glaciations: l'histoire et la stratigraphie des glaciations continentales dans l'hémisphère Nord [The great glaciations: the history and stratigraphy of continental glaciations in the Northern Hemisphere]. Guérin Éditeur Ltée, Montréal (Québec), Canada
Parent M, Occhietti S (1988) Late Wisconsinan Deglaciation and Champlain Sea Invasion

in the St. Lawrence Valley, Québec. Géographie Phys Quat 42:215–246
Pauloo RA, Fogg GE, Guo Z, Henri CV (2021) Mean flow direction modulates non-Fickian transport in a heterogeneous alluvial aquifer-aquitard system. Water Resour Res 57:1–19
Petrelli M (2021) Introduction to Python in Earth Science Data Analysis: From Descriptive Statistics to Machine Learning. Springer International Publishing
Poeter E, Gaylord DR (1990) Influence of Aquifer Heterogeneity on Contaminant Transport at the Hanford Site. Groundwater 28:900–909
Pohlert T (2020) Non-Parametric Trend Tests and Change-Point Detection. https ://creat iveco mmons .org/licen ses/by-nd/4.0/
Possemiers M, Huysmans M, Peeters L, Batelaan O, Dassargues A (2012) Relationship between sedimentary features and permeability at different scales in the Brussels Sands. Geol Belgica 15:156–164
Postma G (1984) Slumps and their deposits in delta fronts and slops. Geology 12:27–30
Prior DB, Bornheld BD, Johns MW (1984) Depositional characteristics of submarine debris flow. J Geol 92:707–727
Rasmussen H, Rouleau A, Chevalier S (2006) Outils de détermination d'aires d'alimentation et de protection de captages d'eau souterraine [Tools for determining well water supply and protection areas]. Ministère du Développement durable, de l'Environnement et des Parcs du Québec, Canada
Ritzi RW, Ghose R, Bottomley M, Reesink AJH, Best J, Freiburg JT, Webb ND (2018) Linking the local vertical variability of permeability and porosity to newly-interpreted lithofacies in the lower Mt. Simon CO2 reservoir. Int J Greenh Gas Control 68:26–41
Robitaille V, Tremblay D (1997) Mécanique des sols, Théorie et pratique [Soil mechanics, theory and practice]. MODULO édition
Rongier G, Peeters L (2022) How fluvial deposits distort charge estmated from groundwater age: Insights from a landscape evolution model. Water Resour Res 58:1–23
Rosas J, Lopez O, Missimer TM, Coulibaly KM, Dehwah AHA, Sesler K, Lujan LR, Mantilla D (2014) Determination of hydraulic conductivity from grain-size distribution for different depositional environments. Groundwater 52:399–413
Roy DW, Tremblay ML, Cousineau PA (2006) Les différents types d'aquifères au Québec [The different types of aquifers in Quebec]. Section 4 dans Outils de détermination d'aires d'alimentation et de protection de captages d'eau souterraine. Rasmussen H, Rouleau A, Chevalier S (eds), Ministère du Développement durable, de l'Environnement et des Parcs, Québec, Canada
Sauerbrey II (1932) On the problem and determination of the permeability coefficient. VNIIG Proc 3–5
Shapiro SS, Wilk MB (1965) An analysis of variance test for normality (complete samples). Biometrika 52:591–611
Singh U, Sharma PK (2022) Comparison of Saturated Hydraulic Conductivity Estimated by Surface NMR and Empirical Equations. J Hydrol. https://doi.org/https://doi.org/10.1016/j.jhydrol.2022.128929
Slomka JM, MacCormack KE, Eyles CH (2019) Preservation of local high-resolution data in a regional low-resolution dataset: A 'nested' 3D modeling approach using an example from a Quaternary glacial stratigraphy (Ontario, Canada). Eng Geol

248:309–329
Sun AY, Ritzi RW, Sims D. (2008) Characterization and modeling of spatial variability in a complex alluvial aquifer: Implications on solute transport. Water Resour Res 44:1–16
Theis, C.V. 1935. The relation between the lowering of the piezometric surface and the rate and duration of discharge of a well using groundwater storage. EOS, Transactions American Geo-physical Union. 16 (2), 519-524.
Tremblay P (2005) Étude hydrogéologique de l'aquifère de Saint-Honoré avec emphase sur son bilan hydrique [Hydrogeologic analysis of Saint-Honoré aquifer with emphasis on its water budge]. Master's Thesis, Université du Québec à Chicoutimi, Québec, Canada
Vukovic M, Soro A (1992) Determination of hydraulic conductivity of porous media from grain-size composition. Water Resources Publications, Littleton, Colorado
Walter J, Chesnaux R, Boumaiza L, Karthikeyan B, Regenspurg S (2023) Conceptual model for the chemical evolution of groundwater in a region of the Canadian Precambrian shield covered by soft Quaternary deposit of glacial and marine origin. Appl Geochemistry. https://doi.org/10.1016/j.apgeochem.2023.105574
Walter J, Rouleau A, Chesnaux R, Lambert M, Daigneault R (2018) Characterization of general and singular features of major aquifer systems in the Saguenay-Lac-Saint-Jean region. Can Water Resour J 43:75–91
Wentworth CK (1922) A scale of grade and class terms for clastic sediments. J Geol 30:507–521
WHO (World Health Organization) (2017) Guidelines for drinking-water quality, 4th edition, incorporating the 1st addendum. ISBN: 978-92-4-154995-0
Winiarski T, Lassabatere L, Angulo-Jaramillo R, Goutaland D (2013) Characterization of the Heterogeneous Flow and Pollutant Transfer in the Unsaturated Zone in the Fluvio-glacial Deposit. Procedia Environ Sci 19:955–964
Won J, Park J, Choo H, Burns S (2019) Estimation of saturated hydraulic conductivity of coarse-grained soils using particle shape and electrical resistivity. J Appl Geophys 167:19–25
Yin M, Ma R, Zhang Y, Lin J, Guo Z, Zheng C (2023) Competitive control of multiscale aquifer heterogeneity on solute transport in an alluvial aquifer. J Hydrol 616:1–13
Zappa G, Bersezio R, Felletti F, Giudici M (2006) Modeling heterogeneity of gravel-sand, braided stream, alluvial aquifers at the facies scale. J Hydrol 325:134–153
Zhang R (1997) Determination of soil sorptivity and hydraulique conductivity from the disk infiltrometer. Soil Sci Soc Am J 61:1024–1030